TÜRKİYE CUMHURİYETİ

ADANA ALPARSLAN TÜRKEŞ SCIENCE AND TECHNOLOGY UNIVERSITY

GRADUATE SCHOOL

MECHANICAL ENGINEERING DEPARTMENT

NATURAL AND FORCED CONVECTION FROM ROTATING TWO TANDEM CYLINDERS POSITIONED IN A CAVITY

Berkay TAŞ

M.Sc.

ADANA 2024

TÜRKİYE CUMHURİYETİ
ADANA ALPARSLAN TÜRKEŞ SCIENCE AND TECHNOLOGY UNIVERSITY

GRADUATE SCHOOL
MECHANICAL ENGINEERING DEPARTMENT

NATURAL AND FORCED CONVECTION FROM ROTATING TWO TANDEM CYLINDERS POSITIONED IN A CAVITY

Berkay TAŞ

M.Sc.

Associate Professor
Nazım KURTULMUŞ

ADANA, 2024

DECLARATION OF CONFORMITY

I would also like to thank my beloved family for their support and motivation. In this thesis study, which was prepared following the thesis writing rules of Adana Alparslan Türkeş Science and Technology University Institute of Graduate School, I declare that I provide all the information, documents, evaluations and results in accordance with scientific ethics and moral codes without resorting to any means or assistance that would be contrary to scientific ethics and traditions. I also declare that I refer to all of the articles I used in this study with appropriate references and accept all moral and legal consequences if a situation is found contrary to my statement regarding my work.

16/07/2024
[Signature]
Berkay TAŞ

ÖZET

KAVİTE İÇERİSİNE KONUMLANDIRILAN İKİLİ VE DÖNDÜRÜLEN SİLİNDİRDEN MEYDANA GELEN DOĞAL VE ZORLANMIŞ TAŞINIM

Berkay TAŞ
Yüksek Lisans, Makine Mühendisliği Anabilim Dalı
Danışman: Doç. Dr. Nazım KURTULMUŞ
Temmuz 2024, 61 sayfa

Bu tez, bir kavite içerisine yerleştirilen iki ısıtılan silindirden meydana gelen doğal ve zorlanmış taşınımın kapsamlı bir incelemesini sunmaktadır. Araştırma, sıcaklık farkları nedeniyle meydana gelen doğal konveksiyon akımları ile akışın ve silindirlerin dönmesinin neden olduğu zorlanmış konveksiyon etkileri arasındaki karmaşık etkileşimi ele almaktadır. Hesaplamalı akışkanlar dinamiği (CFD) simülasyonlarından yararlanarak, elde edilen akış alanı ve ısı transferi oranlarını incelenmiştir. Bulgular, silindirlerin dönüşünün konveksiyon ile ısı transfer mekanizmaları üzerinde derin bir etkiye sahip olduğunu ve bu durumun termal performansı artırdığını ortaya koymaktadır. Özellikle, kavitede meydana gelen akış dinamiklerini önemli ölçüde değiştirerek daha etkili bir termal dağılımı sağlamaktadır. Bu bağlamda, sabit ısı akısına sahip iki silindir, adyabatik duvara sahip havalandırmalı kavitenin merkezine yerleştirilmiştir. Silindirlerin dönmediği veya sürekli olarak aynı veya zıt yönlerde döndüğü senaryolar için simülasyonlar gerçekleştirilmiştir. Ayrıca, silindirler arasındaki mesafe değişimlerinin termal performans ve akış yapıları üzerindeki etkileri de incelenmiştir. Bu çalışmada, Reynolds sayısı 100-300 aralığında, Grashof sayısı ise 10^3 ve 10^5 aralığında değişmektedir. Sonuçlar, silindirlerin döndürülmesinin ısı transfer oranını önemli ölçüde artırdığını göstermiştir. Silindirlerin döndürülmesi durumunda, birinci silindir için yaklaşık %21, ikinci silindir için ise yaklaşık %90 oranında bir ısı transferi artışı gözlemlenmiştir.

Anahtar Kelimeler: Taşınım, Kavite, Silindir

ABSTRACT

NATURAL AND FORCED CONVECTION FROM ROTATING TWO TANDEM CYLINDERS POSITIONED IN A CAVITY

Berkay TAŞ
M.Sc., Department of Mechanical Engineering
Supervisor: Assoc. Prof. Dr. Nazım KURTULMUŞ
July 2024, 61 pages

This thesis presents a comprehensive investigation of the mixed convection phenomena from two hot cylinders situated within a vented cavity. The research addresses the intricate interplay between natural convection currents induced by temperature gradients and forced convection effects resulting from the ventilation of the cavity and the cylinder's rotation. Employing computational fluid dynamics (CFD) simulations, the results meticulously examined the resultant flow field and heat transfer rates. The findings reveal a profound influence of the cylinder's rotation on the convective heat transfer mechanisms, leading to enhanced thermal performance. Notably, the venting configuration significantly alters the flow dynamics, facilitating more effective thermal dissipation. In this context, two cylinders with fixed heat fluxes are positioned at the center of ventilated cavity having adiabatic wall. Simulations have been conducted for scenarios where the cylinders remain stationary or rotate continuously in the same or opposing directions. Furthermore, the effect of variations the space between the cylinders on thermal performance and flow structures have been explored. Reynolds number and Grashof number vary from 100 to 300 and from 10^3 to 10^5, respectively. The results showed that rotating the cylinders significantly improves the heat transfer rate through the cylinders. Upon rotation of the cylinders, an enhancement in heat transfer of approximately 21% is observed for the first cylinder, while the second cylinder exhibits an improvement of about 90%.

Keywords: Cavity, Cylinders, Mixed convection, Natural convection, Forces convection

Dedication

In this thesis work, I would like to thank for his support and motivation to my advisor Assoc. Prof. Dr. Nazım KURTULMUŞ. I would also like to thank my beloved family for their support and motivation.

TABLE OF CONTENTS

LIST OF FIGURES

LIST OF ABBREVIATIONS

Da	: Darcy number
Gr	: Grashof number
Ha	: Hartmann number
Nu	: Nusselt number
Ra	: Rayleigh number
Re	: Reynolds number
Ri	: Richardson number
T_c	: Cold temperature
T_h	: Hot temperature
$\boldsymbol{\omega}$ (rad/s)	: Angular velocity

LIST OF SYMBOLS

Da	: Darcy number
Gr	: Grashof number
H (m)	: Heigth of cavity
Ha	: Hartmann number
Nu	: Average Nusselt number
ω (rad/s)	: Angular velocity
Pr	: Prandtl number
Ra	: Rayleigh number
Re	: Reynolds number
Ri	: Richardson number
Tc	: Cold temperature
Th	: Hot temperature

1. INTRODUCTION

Heat transfer via convection is a prevalent phenomenon observable in various natural processes as well as in diverse industrial applications. As one of the significant modes of heat transfer, convection begins to exhibit variations with the introduction of fluid movement into the process. Free (natural) convection and forced convection represent two distinct processes that differ fundamentally in their physical mechanisms of heat transfer.

Forced convection refers to the heat transfer process that arises due to fluid motion induced by inertial forces, which are influenced by the temperature gradient between the fluid flow and the boundary surfaces, as well as by pressure variations. The inertial and buoyancy forces driving the fluid motion collectively influence the heat transfer dynamics in mixed convection scenarios. The direction of the bulk flow, buoyancy-driven natural convection, and temperature gradients can assume varying roles within the heat transfer process. Free convective flow is classified as auxiliary flow, as both forced and free convection occur in the same direction. Conversely, counterflow involves convective movements that take place in opposing directions, while cross flow is characterized by flow directions that are perpendicular to one another. Transverse and auxiliary flows enhance heat transfer; however, opposing flows can negatively impact the efficiency of heat transfer.

Vented cavity flow presents a significant challenge in mixed convection applications. In this context, the fluid is contained within a confined enclosure, where varying thermal conditions exist at the cavity boundaries, and one or more walls of the enclosure are in motion. The temperature differential between the walls induces natural convection due to fluid movement driven by buoyancy forces. The no-slip condition is maintained at the moving boundaries within the enclosure, leading to circulation induced by wall motion. Consequently, this circulation facilitates heat transfer through forced convection within the cavity.

2. THEORETICAL FOUNDATIONS AND LITERATURE REVIEW

Hamzah et al. (2021) investigated the flow characteristics and entropy generation of a hot cylinder positioned between two counter-rotating cylinders within a ventilated cavity. The investigation centers on mixed convection in a steady, two-dimensional, laminar flow regime. Two vertical and three horizontal distances from the heated cylinder are analyzed, with angular rotational speeds (Ω) varying from 0 to 15. Reynolds number varying from 100 to 500 changes and Grashof number ($10^3 \leq Gr \leq 10^6$) variations are considered. It was demonstrated that the positioning of the counter-rotating cylinders significantly affects both hydrothermal dynamics and entropy production within the cavity. An increase in the Reynolds number provides higher average Nusselt numbers and average entropy generation though this is also associated with a rise in pressure drop.

Ouri et al. (2023) examines convective heat transfer and phase change in an L-shaped ventilated cavity with a rotating cylinder and a phase change material-packed bed (PCM-PB) system under a magnetic field with hybrid nanofluid as a working fluid. Numerical simulations assessed various parameters, including Reynolds number, rotational Reynolds number, cylinder size, and Hartmann number, with a fixed nanoparticle concentration of 2% Ag/MgO in water. Findings revealed that adjusting cylinder size, speed, and magnetic field strength can control vortex size and distribution. The cylinder's rotation direction also affects phase transition dynamics, increasing transition time by up to 27% compared to a stationary cylinder.

Battira et al. (2023) conducted a numerical analysis of forced convection within an adiabatic square ventilated enclosure that incorporates a rotating heated hexagonal cylinder. The forced flow of a water-copper nanofluid is oriented perpendicular to the axis of the cylinder. The research examines Reynolds numbers varying from 200 to 1000, rotational Reynolds numbers varing from -30 to 30), nanoparticle volume fractions varying from 0 to 3%, and the rotational direction of the hexagonal cylinder, on the enhancement of heat transfer. In the stationary condition of the cylinder, a 50% increase in the inlet velocity of the nanofluid leads to an 18.56% improvement in heat transfer rates. The lowest average Nusselt number occurs when the cylinder remains stationary; however, as the rotational speed of the cylinder increases, the heat transfer rate improves. Notably, this enhancement is approximately equal for both directions of rotation of the hexagonal cylinder.

Selimefendigil and Öztop (2023) investigated the dynamics of phase change processes within a multi-vented cavity system featuring encapsulated phase change materials (PCMs), with a particular focus on the influence of rotating cylinders and magnetic fields, numerically. The study employs numerical simulations to analyze various influencing factors, including rotational Reynolds numbers (Re_w) ranging from 0 to 10000, the spacing between cylinders, magnetic field strength represented by the Hartmann number (Ha from 0 to 50), and the size of the inlet port. The results indicate that phase change processes are slower for Rew values up to 6,000, after which the rate accelerates.

Omar and Ali (2023) investigated the dynamics of mixed convection of two horizontally aligned cylinders within a vented square enclosure characterized by openings on the upper and lower surfaces numerically. Key parameters analyzed include the dimensions of the openings, the spacing between the cylinders, Richardson numbers varying from 0.1 to 10, and Reynolds numbers varying from 50 to 400, while maintaining a constant Prandtl number (Pr = 0.72). The results indicate a significant correlation between the average Nusselt number (Nu) and variations in Richardson number, Reynolds number, and opening dimensions. Specifically, increasing the spacing to 0.375 leads to a notable enhancement of the average Nu surrounding the heated cylinder. Overall, the average increase in Nu is observed to range from 10% to 38%.

Azad et al. (2023) investigated numerically hydrothermal characteristics in a partially heated square enclosure containing a rotating cylinder, specifically under a magnetic field and using CNT-water nanofluid as working fluid. Numerical simulations were performed to evaluate the impact of varying rotational speeds and dimensionless times on thermal and fluid flow dynamics. The research highlights that increasing rotational speed significantly increases the drag force on the cylinder surface. In general, improved fluid flow and thermal performance are associated with increased cylinder rotation speeds.

Selimefendigil and Öztop (2024) investigated mixed convection in a magnetically influenced cavity with lid driven configuration. Various parameters are analyzed. Experimental validation for mixed convection in a lid-actuated cavity is also performed. The results show that the effect of chamber rotation becomes important when natural convection effects dominate.

Khanafer and Aithal (2013) investigated mixed convection in a cavity with a circular cylinder. The upper and lower walls are seen to be maintained at low and high temperatures, whereas the right and left walls are thought to be adiabatic. Consequently, the Nusselt number rise in a cavity with cylinder comparatively to the cavity without a cylinder. Increasing the Richardson number in this process and analysis also raises the average Nusselt number.

The main topic of study for Khanafer and Chamkha (1999) is mixed convective flows in a cavity with fluid-saturated porous media. This application involved the calculation of momentum, continuity, and energy equations as well as the use of the ADI (Alternative Direct Implicit) method and the eddy current function. The corresponding flow field variation in the porous media within the housing is computed by incorporating the momentum and energy equations of the Brinkmann-Darcy equation. The study examined the numerical outcomes of a fluid's mixed convective heat transfer when it operates in a porous medium and produces heat in a vacuum. The Gr/Re^2 ratio, the internal Rayleigh number, Ra, and the Darcy number, Da are the dimensionless control parameters in research. The Darcy and Richardson numbers' effects are displayed.

Khanafer and Chamka (1998) investigated the substantial effect of Richardson number, Ri on the flow field and heat transfer in a gap. For small Ri, forced convection has been shown to be superior in the heat transfer process. Natural convection gains significance as Ri increases, and it is also claimed that convection diminishes as a result of mass movement because of the porous medium's friction factor. The limited fluid movement within the housing causes the heat transfer between the top and bottom walls to converge to pure conduction because of the low permeability of small Darcy numbers.

Alleborn et al. (1999) studied numerically fixed two-dimensional configurations with heat and mass transfer in a flat cover gap with corresponding moving heated cover and moving cooled cover. Mathematical results are compared with analytical solutions for the boundary states of geometric parameters obtained through computer algebra. The dependence of the mass and heat transfer rates on wall velocities and different concentration boundary conditions was examined in a parametric study of the cavity's vertical and horizontal tendency. The research yielded data on vibration regimes with minimal heat and mass transfer in a vertical cavity, as well as two inflection points, the configuration's beginning point, and a horizontal cavity heated below the Hopf bifurcation. Additionally, this study examined an idealized double-walled flat cavity that moved in its own plane and contained a mixture of gaseous solvent vapors as a means of extracting solvents from a liquid situated in a moving network.

Khanafer and Vafai (2002) conducted a study on fluid flows induced by buoyancy effects on convection, also referred to as thermoisolated convection, which are influenced by temperature and concentration gradients. Crystal growth is a natural and technological phenomenon with applications in thermal insulation, solar energy systems, and welding processes. Previous research has primarily focused on mass and heat transfer in solid-walled enclosures. By taking into account various factors such as aspect ratio, Reyleigh number, and Prandtl number, effective boundary conditions for temperature and flow fields in the aperture plane of the two-dimensional structure were established. A thorough analysis was carried out to compare the average Nusselt number between the two models, confirming the validity of the current effective boundary conditions.

Costa and Raimundo (2010) was investigated mixed convection mathematically using a rotating cylinder within a square closed region. The rotational motion of the cylinder in conjunction or opposition determines the effect of both forced and natural convection. Due to the nature of mixed flow, the combined effects may not always result in the enclosure transferring heat as well as possible. The heat transfer processes of convection and conduction are combined in the rotating cylinder. Therefore, in addition to thermal conductivity and heat capacity, the mixed convection problem of the cylinder radius was also investigated. The total Nusselt number was used to analyze the thermal performance of the package. Six dimensionless parameters, including Reyleigh Ra number, Prandtl Pr number and dimensionless velocity, control this system. The cylinder is positioned at the center of the housing. Findings showed that the fluctuations in temperature and pressure have no effect on the density of the liquid. Temperature affects density.

In the study carried out by Mahmud et al. (2022), the internal heat generation and mixed convection heat transfer of a centrally rotating isothermal cylinder in a lidded square chamber were studied. The upper part of the chamber can be moved while the lower part remains stationary while the cylinder rotates clockwise at a fixed speed. The temperature in the room is heated evenly. In the parametric simulation, constant velocity Reynolds numbers varying from 31.623 to 316.23, Grashof numbers varying from 10^3 to 10^5, Richardson numbers varying from 0.1 to 10. The upper part of the chamber remains at temperature T_c while sliding in the positive X direction at a constant speed of u_0. On the other hand, $T_h>T_c$ and the bottom wall is kept at a constant temperature. Its two side walls are both immovable and insulated. In the center of the room (L/2, L/2), there is a circular cylinder with diameter, *D* that rotates clockwise with speed. A constant temperature T_c is maintained on the outside of the cylinder. The air in the room has a Prandtl number of Pr = 0.7.

Billah et al. (2011) used a heated circular hollow cylinder with a cavity. This is a heated, circular hollow cylinder with diameter and thermal conductivity, which is located in the center of a housing with square sides. T_c is the fixed temperature of the sidewalls. On the left vertical wall of the adiabatic space, the upper and lower walls move upward at a constant speed, while the other walls remain constant. The direction of gravity is negative y. Furthermore, it is assumed that the Boussinesq approximation is valid and that radiation, pressure work and viscous dissipation are all negligible. Numerical indicators show the average temperature of the liquid inside the casing, isotherms, the influence of the Nusselt number on the hot wall and the influence of Reynolds, Richardson and Hartmann numbers on streamlines. In addition to the lid-driven cavity effect, the effects of Reynolds number, Joule heating and the central heat-conducting circular block on mixed convection were found.

Costa and Raimundo, (2010) investigated the mixed convection of a centered rotating cylinder within a square closed surface using numerical methods. The effects of forced and natural convection can act in parallel or against each other depending on the rotation pattern of the cylinder. The rotating cylinder performs natural heat exchange with the liquid, which has no surface heat state and participates in convective and conductive heat transfer processes. How the mixed convection problem is affected by the radius, thermal conductivity, rotation speed and heat capacity of the cylinder was studied. The overall thermal performance of the case is examined using the Nusselt number. The local heat exchange between the fluid and the cylinder surface is studied to gain a clear understanding of the role of the cylinder in the heat transfer process. The results show how the thermal performance of the casing is affected by the rotating cylinder and highlight the importance of the thermophysical properties of the cylinder in the overall heat transfer process of the casing.

Hamzah et al (2022) conducted a study on mixed convection within a massive circular cylinder. In numerical analysis, the coupling of structural deformation and fluid flow is used to simulate and solve two-dimensional equations using Galerkin finite elements and the Lagrange-Euler method. The percentage of average Nusselt number increased to 40% at Ri= 0.1 and to 59% at Ri = 200 as Re increased from 50 to 250.

Ali et al. (2024) investigated the use of copper-water nanofluid to transport an annular concentric cylinder. The amplitude and wave number of the cylinder are different. Thus, while increasing the nanoparticle volume fraction and Rayleigh number improves the heat process, increasing the Reynolds number and wave number decreases heat transfer.

The most important results of the current research are:

1. Increasing Richardson and Reynolds numbers to increase and improve fluid flow and heat conduction,

2. The change of time steps affects the continuous change of fluid flow density.

3. In enclosures without baffle plates, the heat transfer rate increased by 18.34%,

4. When the Cauchy number is low, there is no yaw deformation,

Hussain and Hussein (2010) conducted a numerical simulation to solve the problem of laminar steady convection in a two-dimensional square enclosure and a rotating circular cylinder with radius. The finite volume scheme was used in this simulation. In the enclosure where the left side wall is exposed to a higher isothermal temperature than the right side wall, mixed convection was analyzed. The examined housing wall had an air-filled Prandtl number of 0.71 and the upper and lower housing walls were considered adiabatic. Reynolds numbers range from 50 to 300, while Richardson numbers range from 0 to 10. The average Nusselt number is determined by combining these values with thermal fields and fluid flow. According to the study's findings, flow and temperature loss were significantly influenced by increasing Reynolds and Richardson numbers as well as the locations of the rotating cylinders. The present example is a two-dimensional enclosure with a square shape and the same width and height. The outcomes of the study are outlined as follows:

1. Vortices of nearly uniform size are generated around the circular cylinder. Concurrently, forced convection impacts are identified within small eddies situated at the corners of the square enclosure.

2. Maintaining a constant Richardson number results in no alterations in the position of the rotating circular cylinder and the associated flow regions. This absence of change is attributed to the condition Ri = 0.

3. The escalation in the Richardson number influences both thermal and flow domains.

4. An elevation in the Richardson number provide an enhancement in the circulation of flow eddies. These enhancements contribute to an increased prevalence of forced convection effects.

5. The escalation in Richardson and Reynolds numbers, coupled with the placements of the circular cylinders, leads to a corresponding augmentation in the magnitude of the Nusselt number.

Selimefendigil et al. (2014) conducted an investigation on a square enclosure containing a nanofluid-filled lid with mixed convection. The lower wall was heated, while the upper wall was maintained at a lower constant temperature. The study considered the Richardson number varying from 0.001 to 10, Hartmann number varying from 0 to 50, solid volume fraction of nanoparticle varying from 0 to 0.05, and angular rotation speed of the cylinder varying from 10 to 10. A 17% difference in heat transfer was observed when comparing the flow between Ri =

1 and Ri = 10. Increasing the Hartmann number led to a reduction in heat transfer, while increasing the solid volume fraction of the nanoparticle resulted in an increase in heat transfer. The height of the square space was denoted as H, and the diameter of the circular cylinder placed at its center was 0.25H. The upper horizontal wall of the space moved upwards with constant speed, and the cylinder rotated with a constant angular rotation. The no-slip boundary condition was applied to the other walls, with the temperature of the upper wall being T_c and the temperature of the lower wall being T_h. Adiabatic boundary conditions were assumed on the other walls of the cavity and on the cylinder surface. The thermophysical properties of the fluid were considered constant, except for the density change, which was modeled by the Boussinesq approximation. The weak version of the fundamental equations was obtained using the Galerkin approximation. Several numerical runs with different grid sizes were tested to determine the influence of a vertical magnetic field on Cu-water nanofluid (solid volume fraction = 0.2) poured into the square container. When the rotation X value was positive, the cylinder rotated counterclockwise.

The results obtained from the numerical simulation provide the following conclusions:

• Enhancing the Richardson number improves heat transmission. A 17% increase in heat transfer is observed at R_i = 10 compared to Ri = 1.

• The presence of a magnetic field slows down the velocity field and convection, leading to a decrease in average heat transfer as the Hartmann number increases.

• Magnetic fields can be used to control local heat transfer by directing heat transmission towards the right end of the bottom wall.

• An increase in the solid volume percentage of nanoparticles results in improved heat transfer due to the enhanced effective thermal conductivity of the nanofluid, thereby enhancing thermal transport of the fluid.

The properties of nanofluids are significantly improved by nanopowder forms, as demonstrated by Yan et al. (2022) in their study, the impact of nanopowder shape on the irreversibility and natural convection of water/alumina nanofluids was investigated through numerical analysis. A square enclosure with uniform cold (T_c) and hot (T_h) temperatures on the right and left walls, respectively, was utilized for this purpose. The research employed the control volume method to discretize the differential equations, and the conservation form of the equation was integrated across the cells. Algebraic forms of the equations were then introduced, and integrals were computed. If the anticipated pressure distribution is accurate, the calculated velocity field should satisfy the continuity equation. Otherwise, adjustments may be necessary to the predicted pressure distribution values. Consequently, the pressure field can be adjusted by imposing a correction derived from the continuity equation. The continuity, momentum, and energy equations were discretized using the finite volume approach. The outcomes revealed the maximum heat transfer rate and entropy generation of the model. An important discovery highlighted in this paper was that the addition of nanopowder does not always enhance the free heat convection in nanofluids; on the contrary, in certain scenarios, the inclusion of nanopowder can lead to a significant increase in the viscosity of the nanofluid, resulting in reduced irreversibility and Nu number. Furthermore, it was observed that Nu rises with Ra and decreases with the intensity of the magnetic field.

The key findings are as follows:

• The average Nusselt number is increased by 5.8, 5.87, and 5.75, respectively, when utilizing straight, angled, and curved fins and increasing the Rayleigh number from 10^3 to 10^6,

• The entropy production within the enclosure rises with an increase in Rayleigh number and a decrease in Hartmann values,

• Heat transfer decreased by 38%, 40%, and 40% for straight, angled, and curved fins, respectively, with an increase in the Hartmann number,

• The inclusion of nanoparticles with shapes like bricks, fins, platelets, and cylindrical particles in a specific order resulted in the highest heat transfer rates for water,

• Brick-shaped nanoparticles were effective at volume fractions exceeding 1%, while blade, cylindrical, and platelet-shaped nanoparticles at any volume fraction reduced the average Nusselt number and entropy production,

• Research indicated that the addition of a slanted fin improved heat transfer in nanofluids with natural convection, while a high-strength magnetic field led to a similar reduction in heat transfer across all configurations. Ultimately, the angled fin, arced fin, and straight fin were found to offer the most efficient heat transfer, in that order, when selecting the most suitable fin for heat transfer

In this investigation conducted by Öztop et al. (2012), the focus is on the second law analysis of thermodynamics in enclosed spaces due to buoyancy-induced flow in energy systems. The research delves into the realm of mixed transport phenomena. The study of thermodynamic optimization, also referred to as entropy production minimization or EGM, is situated at the crossroads of fluid mechanics, engineering thermodynamics, and heat transfer. Entropy serves as a distinguishing factor between reversible and irreversible processes. The quality of energy can be quantified through its analysis. The efficacy of the first law of thermodynamics is notably restricted in heat transfer engineering systems. Consequently, computations based on the second law of thermodynamics concerning entropy production are deemed more dependable than those based on the first law. The comparison of the actual thermal efficiency under identical conditions can be utilized to ascertain the second law efficiency in nearly any thermal system. Hence, the examination of irreversibility in terms of entropy production rate was carried out using the second law of thermodynamics. It is a well-established fact in thermodynamics that heat transfer results in entropy generation, thereby inducing thermodynamic irreversibility within the system. One approach to optimizing thermodynamic imperfections and fluid flow irreversibility is through entropy minimization. Consequently, it is imperative to explore the generation and reduction of entropy in heating systems to encompass irreversibility in thermodynamic investigations. A high-entropy system, in contrast to a low-entropy system, is characterized by greater disorder or chaos. The primary insight gleaned from the literature review is that heat conduction and fluid friction in a buoyant thermal system are the primary sources of entropy generation. The comprehension of entropy production is crucial for conserving energy and managing heat transfer and fluid flow in all thermal systems. The Rayleigh number emerges as a pivotal metric in the context of entropy generation in natural convection.

Abo-Elkhair et al. (2021) conducted a study to examine the impact of high and low Reynolds number applied magnetic fields on the flow of hybrid bio-nanofluid in a peristaltic channel. The study focused on magnetic force and nonlinear thermal radiation, considering copper and gold nanoparticles. The Adomian decomposition approach was utilized to derive equations for velocity, induced magnetic field components, magnetic pressure, flow function, magnetic force, joule heating, shear stress, and Nusselt number. Plots and analyses were carried out to assess the influence of various physical and biomedical parameters on the aforementioned variables. The results indicated that the hybrid nanofluid exhibited a significant magnetic force, with gold nanofluid displaying the highest velocity among the basic, hybrid, and copper nanofluids. The study aimed to investigate the effects of applied magnetic fields on the system.

Yaseen et al. (2023) conducted a study to analyze transient entropy production and mixed convection due to a rotating, heated inner cylinder within a square cavity with a flexible side wall. The study explored the impact of several key factors on dimensionless time, including Rayleigh number varying from 10^4 to 10^7, angular rotation rate varying from -1 to 1, and dimensionless elasticity. The research presented a 2D transient laminar mixed convection flow for a viscous incompressible Newtonian fluid in a square space with side, featuring a heated, rotating circular cylinder of radius and temperature at the center of the cavity. The right wall was assumed to be flexible, while the left wall was rigid, with both vertical walls maintained at a constant cold temperature. Insulation was applied to the horizontal wallsThe findings revealed that different complex wall deformations are generated based on the rotation direction of the cylinder and the dimensionless elastic modulus of the flexible right wall. Additionally, Ra was found to increase the local and average Nusselt numbers, with secondary peaks in the local Nusselt number occurring at lower Ra values. Counterclockwise rotating circular cylinder and lower flexible wall deformation were associated with the highest average heat transfer and global entropy production rates. The study also suggested that mixed convection is more intricate than other forms of convection due to the combined effects of shear force from wall motion and buoyancy from temperature difference.

This study investigates the phenomenon of mixed convection from two rotating/stationary cylinders placed within a square cavity. The distance between the cylinder's variation of two cylinders along the x-axis is specifically investigated. The effect of the rotation of these cylinders on heat transfer and flow structures also exmied. The primary focus is on analyzing how variations in the Grashof number (Gr) and Reynolds number (Re) impact both heat transfer characteristics and flow patterns within this complex fluid dynamics scenario.

3. MATERIAL AND METHODS

3.1. Model Descriptions

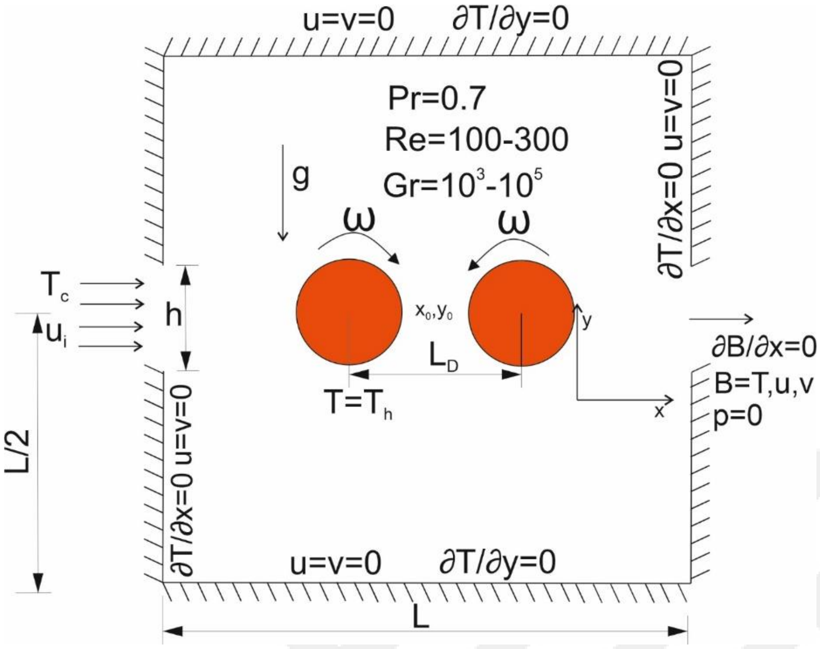

Figure 1. The model of vented cavity with boundary conditions

Figure 1 shows the model of the geometry in this study. The center of two stationary/rotating cylinders are located at centerline of the Cartesian coordinate system. The length of a side of the cavity is represented by L. L_D represents the distance between the cylinders. The diameter of a cylinder is represented by D. The outlet and inlet are symmetrical with respect to the center of the Cartesian coordinate system. Their length, *h* is assumed as L/5. The cavity walls are treated as adiabatic. A working fluid which is air introduce the cavity from the inlet as uniform at cold temperature, T_c. The heated cylinders' walls are kept at a hot temperature, T_h. The diameter of a cylinder is taken as L/5. The distance between the cylinders, L_D/D varies between 1.5 and 3. No-slip condition has applied to the walls of the cavity and cylinder. The heated cylinders can be at stationary or can rotate. Four cases are considered for the rotation such as first cylinder (situated near the inlet) rotates counterclockwise and second cylinder (situated near the outlet) rotates clockwise, first cylinder rotates clockwise and second cylinder rotates counterclockwise, both of them rotates clockwise and both of them rotates counterclockwise. Additionally, two different angular velocity are considered for the rotation.

3.2. Governing equations and solution procedure

In this study, the flow is characterized as incompressible, two-dimensional, laminar and at a steady state. The Prandtl number is set at 0.7. The thermophysical properties of air are considered constant, with the exception of density, for which the Boussinesq approximation is employed. Furthermore, the effects of radiation and viscous dissipation are deemed negligible. The governing equations for the system are delineated as follows:

Continuity equation,

$$\frac{\partial u}{\partial x} + \frac{\partial v}{\partial y} = 0 \tag{1}$$

Momentum equations,

$$u\frac{\partial u}{\partial x} + v\frac{\partial u}{\partial y} = -\frac{1}{\rho}\frac{\partial p}{\partial x} + \frac{\mu}{\rho}\left(\frac{\partial^2 u}{\partial x^2} + \frac{\partial^2 u}{\partial y^2}\right) \tag{2}$$

$$u\frac{\partial v}{\partial x} + v\frac{\partial v}{\partial y} = -\frac{1}{\rho}\frac{\partial p}{\partial x} + \frac{\mu}{\rho}\left(\frac{\partial^2 v}{\partial x^2} + \frac{\partial^2 v}{\partial y^2}\right) + \beta g(T - T_c) \tag{3}$$

Energy equation,

$$\left(u\frac{\partial T}{\partial x} + v\frac{\partial T}{\partial y}\right) = a\left(\frac{\partial^2 T}{\partial x^2} + \frac{\partial^2 T}{\partial y^2}\right) \tag{4}$$

where $a = k/\rho c_p$' dir.

The dimensionless parameters are as follows,

X=x/L, Y=y/L, $V=\frac{v}{u_i}$, $U=\frac{u}{u_i}$, $\theta = \frac{T-T_c}{T_h-T_c}$, $Re = \frac{u_i L}{\vartheta}$, $Gr = \frac{g\beta(T_h-T_c)L^3}{\vartheta^2}$, Pr = ϑ / a

The local Nusselt number, Nu_y can be calculated as follows,

$$Nu_y = -\left(\frac{\partial\theta}{\partial Y}\right)_{Y=0} \tag{5}$$

The average Nusselt number, Nu_{avg} can be calculated as follows,

$$Nu_{avg} = \frac{1}{L}\int_{X=0}^{X=L} Nu_y dX \tag{6}$$

The boundary conditions at the inlet are U=1, V=0 and $\theta = 0$

The boundary conditions at the outlet are $\frac{\partial U}{\partial X} = 0$, $\frac{\partial V}{\partial X} = 0$ and $\frac{\partial\theta}{\partial X} = 0$ and P=0

The boundary conditions at the cavity wall are U=0, V=0 and $\frac{\partial\theta}{\partial X} = 0$

The boundary conditions for a heated cylinder are U=0, V=0 and $\theta = 1$ when it is stationary.

The boundary conditions for a heated cylinder are U=−Ω ($Y - Y_o$), V=−Ω ($X - X_o$), $\theta = 1$ when it is rotary.

Where Ω represents the dimensionless angular rotational velocity and it is calculated as $\Omega = \frac{wL}{2U_i}$.

A commercial computational fluid dynamics (CFD) solver, Ansys Fluent (2018), was utilized to investigate the problem at hand, employing the finite volume method. A straightforward algorithm was implemented, and the second-order upwind scheme was adopted. Iterative calculations were conducted until the convergence criterion of 1×10^{-8} was satisfied.

A validation study was undertaken, demonstrating that the findings of the current investigation are consistent with the results obtained by Lee et al. [25], who analyzed convection from a hot cylinder within a cavity. In their research, the heated cylinder was situated within a square enclosure under isothermal boundary conditions. For the validation case, a Rayleigh number of 10^5 was specified, resulting in a mean Nusselt number of 7.76. The present study, under identical boundary conditions, yielded a mean Nusselt number of 7.86, indicating a difference of only 1%.

4. ANALYSIS AND DISCUSSION

4.1 Heat Transfer Results

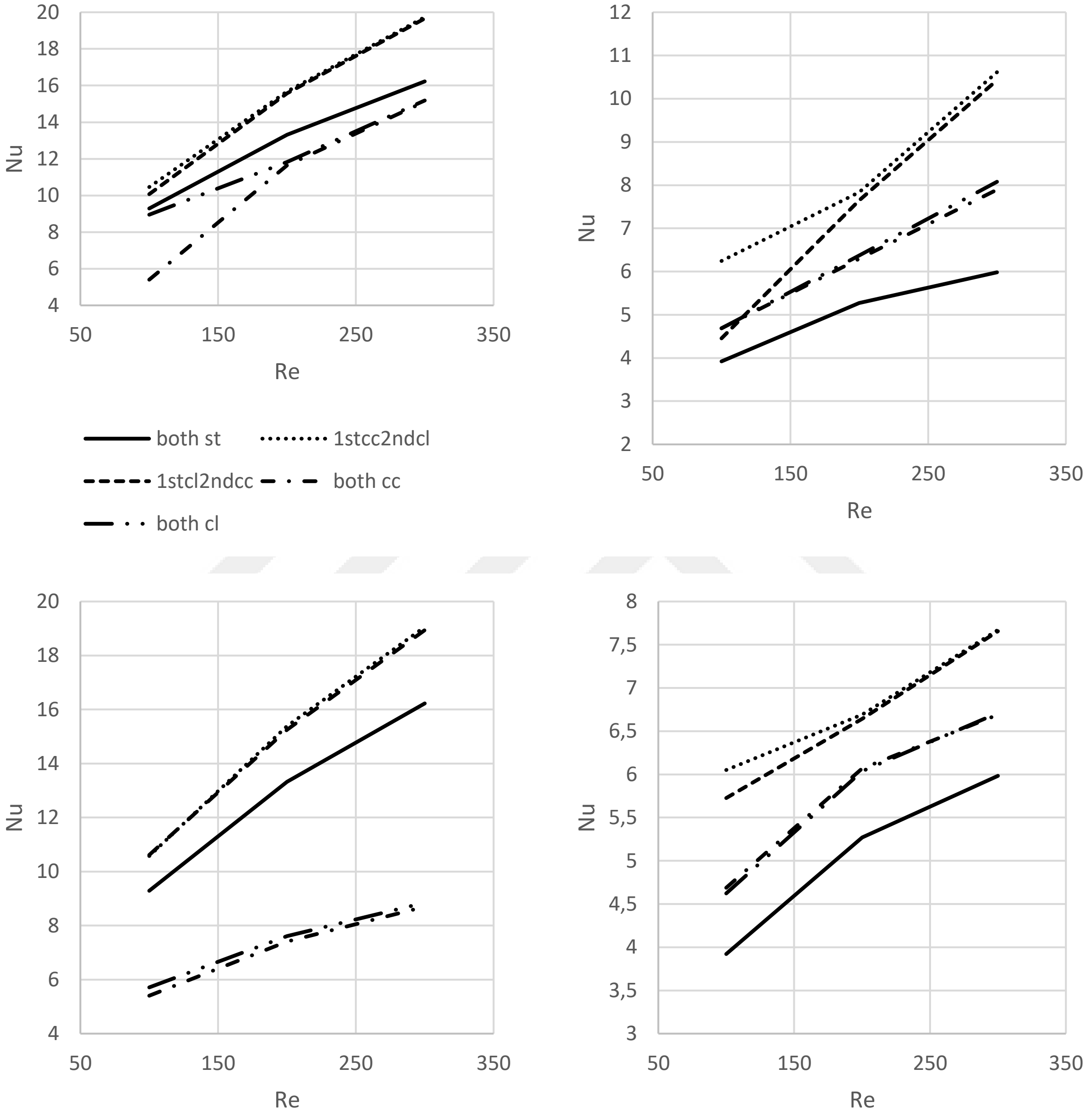

Figure 2. Nu number, Nu variations with increasing Reynolds number, Re at Gr=10^3, L_D/D =1.5

The Nusselt number, *Nu* variations with increasing Reynolds number, *Re* are shown for the cylinders located in a cavity are seen in Figure 2-13. In these figures, as the results at first row belongs to the case of cylinders with angular rotational velocity, Ω =6, the results at second row belongs to the case of cylinders with angular rotational velocity, Ω =12. And as the results at first column belongs to only first cylinder, the results at second column belongs to only second cylinder.

Figure 2 shows the Nusslet number variations, *Nu* variations with increasing Reynolds number, Re at $Gr=10^3$, L_D/D =1.5. In all cases for L_D/D =1.5, the Nusselt number increases with increasing Reynolds number including stationary cylinders as seen at Figure 2. In the case that the first cylinder rotates counterclockwise, and the second cylinder rotates clockwise shows that the Nusselt number associated with the first cylinder is higher compared to when both cylinders are stationary. The maximum Nusselt Number, *Nu* for first cylinder is obtained as 19.66 for the case of the first cylinder rotates counterclockwise and the second cylinder rotates clockwise at Re=300 and Ω =6. Conversely, when both cylinders rotate counterclockwise or clockwise, the Nusselt number for the first cylinder is clearly lower than both cylinders were stationary. Rotation of the cylinders increases the calculated Nusselt number, *Nu* for the second cylinder in all cases. The maximum Nusselt Number, *Nu* for second cylinder is obtained as 10.42 for the case of the first cylinder rotates counterclockwise and the second cylinder rotates clockwise at Re=300 and Ω =6. The maximum Nusselt Number, *Nu*, for the second cylinder is obtained as 10.4 when the first cylinder is rotating clockwise, and the second cylinder is rotating counterclockwise at Re=300 and Ω=6. While increasing the angular velocity does not affect the Nusselt numbers, *Nu* obtained from the first cylinder much, the Nusselt numbers, *Nu* obtained from the second cylinder mostly decreases.

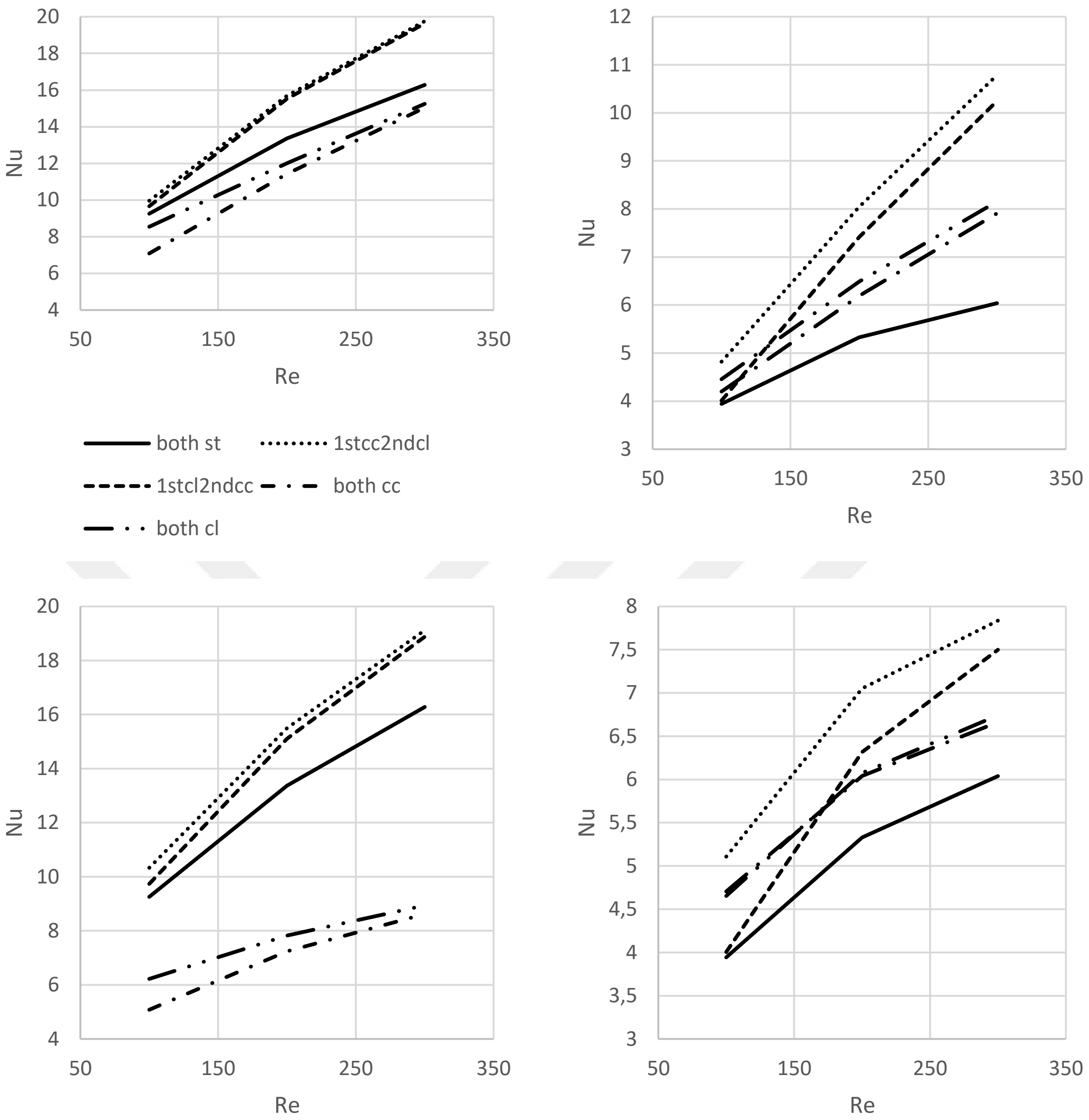

Figure 3. Nu number, Nu variations with increasing Reynolds number, Re at Gr=10^4, LD/D =1.5

Figure 3 shows the Nusselt number variations, *Nu* variations with increasing Reynolds number, Re at Gr=10^4, $L_{D/}D$=1.5. In the case that the first cylinder rotates counterclockwise, and the second cylinder rotates clockwise shows that the Nusselt number associated with the first cylinder is higher compared to when both cylinders are stationary. The maximum Nusselt Number, *Nu* for first cylinder is obtained as 19.63 for the case of the first cylinder rotates counterclockwise and the second cylinder rotates clockwise at Re=300 and Ω =6.

Conversely, when both cylinders rotate counterclockwise or clockwise, the Nusselt number for the first cylinder is clearly lower than if both cylinders were stationary. Rotation of the cylinders increases the calculated Nusselt number, Nu for the second cylinder in all cases. The maximum Nusselt Number, *Nu* for second cylinder is obtained as 10.78 for the case of the first cylinder rotates counterclockwise and the second cylinder rotates clockwise at Re=300 and Ω =6. The minimum Nusselt number, *Nu* is obtained as 5.08 for the case of both cylinders rotating counterclockwise at Re=100 and Ω =12 in all cases of L_D/D=1.5.

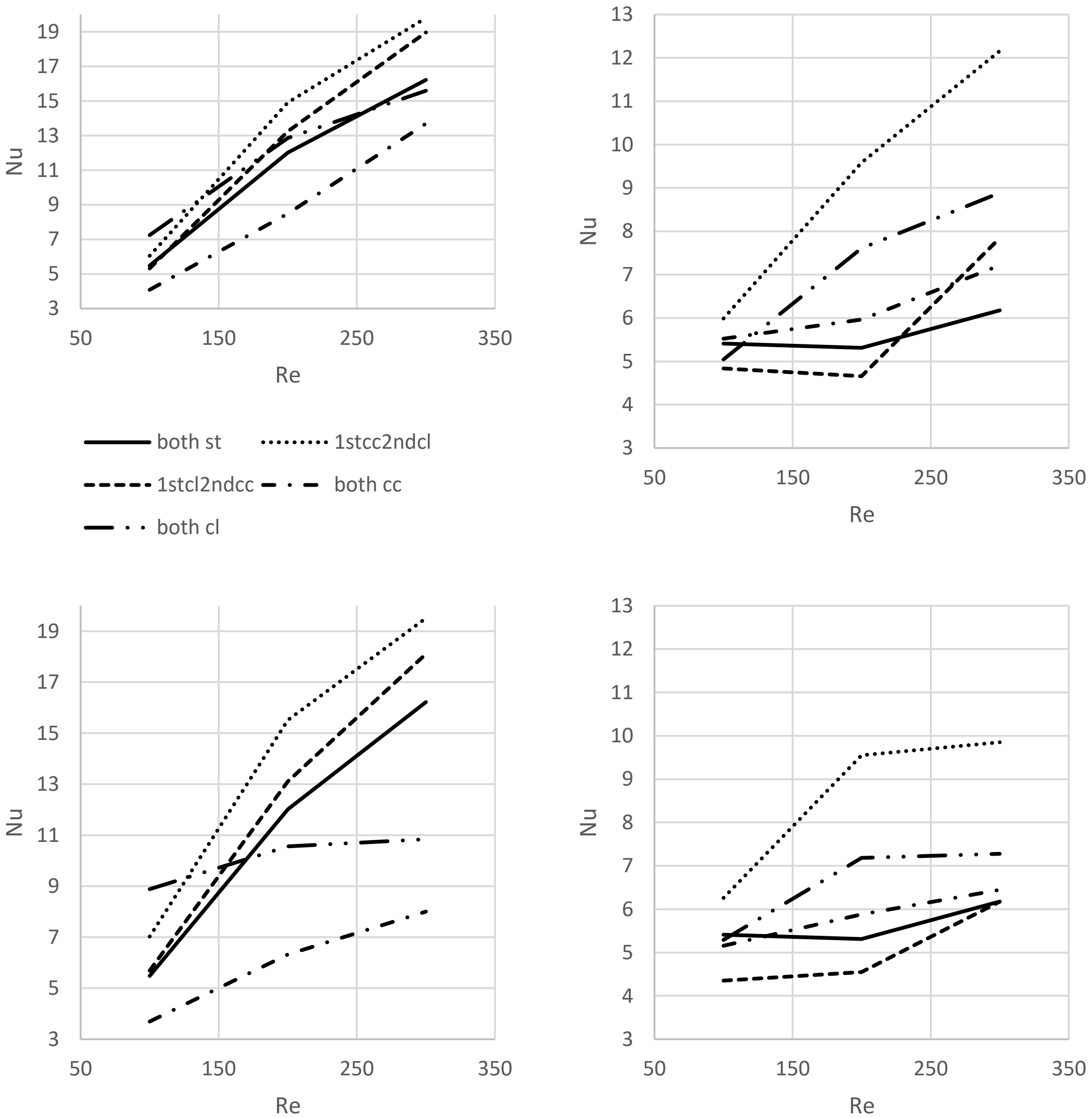

Figure 4. Nu number, *Nu* variations with increasing Reynolds number, Re at Gr=10^5, L_D/D =1.5

Figure 4 shows the Nusselt number variations, *Nu* variations with increasing Reynolds number, Re at Gr=10^5, L_D/D =1.5. When the first cylinder rotates counterclockwise and the second cylinder rotates clockwise, the Nusselt number associated with the first cylinder is found to be higher than when both cylinders are at stationary. The maximum Nusselt Number, *Nu*, for the first cylinder is obtained as 19.80 when the first cylinder is rotating counterclockwise, and the second cylinder is rotating clockwise at Re=300 and Ω=6. Conversely, when both cylinders are rotating counterclockwise or clockwise, the Nusselt number for the first cylinder is clearly lower than when both cylinders are at stationary. The rotation of the cylinders increases the Nusselt number, *Nu*, calculated for the second cylinder in almost all cases. The maximum Nusselt number, Nu, for the second cylinder is obtained as 12.15 when the first cylinder is rotating counterclockwise, and the second cylinder is rotating clockwise at Re=300 and Ω=6. The minimum Nusselt number, *Nu* is obtained as 3.69 for the case of both cylinders rotating counterclockwise at Re=100 and Ω =12 in all cases mentioned in Figure 4.

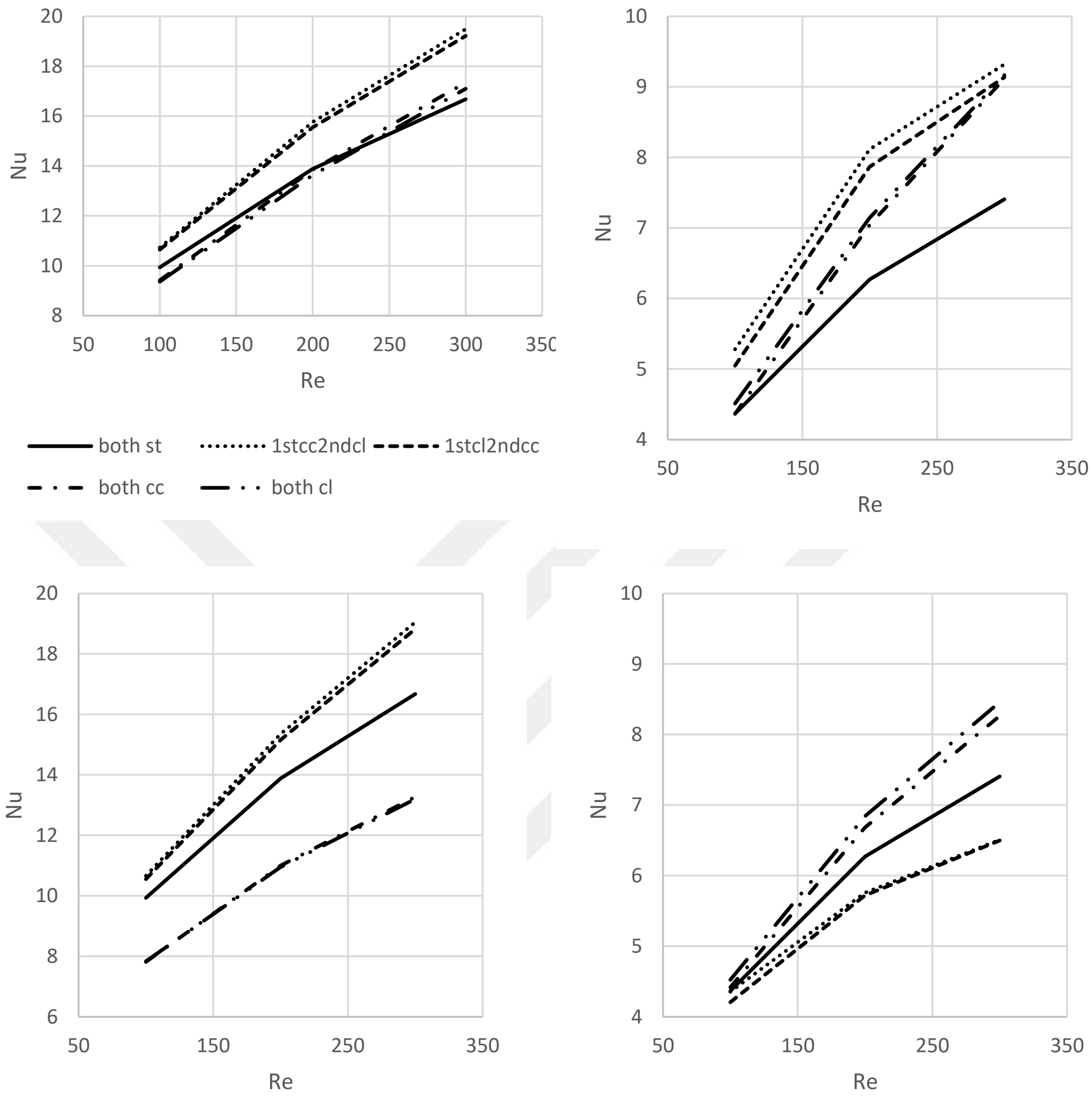

Figure 5. Nu number, *Nu* variations with increasing Reynolds number, Re at Gr=10^3, L_D/D =2 for different configurations.

Figure 5 shows the Nusselt number variations, *Nu* variations with increasing Reynolds number, Re at Gr=10^3, L_D/D =2. When the first cylinder rotates counterclockwise and the second cylinder rotates clockwise, the Nusselt number associated with the first cylinder is found to be higher than when both cylinders are at stationary. The maximum Nusselt Number, *Nu*, for the first cylinder is obtained as 19.21 when the first cylinder is rotating counterclockwise, and the second cylinder is rotating clockwise at Re=300 and Ω=6. As the rotation speed increases, a decrease in the heat transfer rate from the second cylinder is observed. For instance, the Nusselt Number, *Nu*, for the second cylinder is obtained as 6.49 at Ω=12 for the same cases, namely, when the first cylinder is rotating counterclockwise, and the second cylinder is rotating clockwise at Re=300 and Ω=6. Moreover, the minimum Nusselt number occurs at high rotational velocities. For example, the minimum Nusselt number, Nu is obtained as 4.2 for the case when the first cylinder rotates clockwise and the second cylinder rotates counterclockwise at Re=100 and Ω =12 in all cases mentioned in Figure 5.

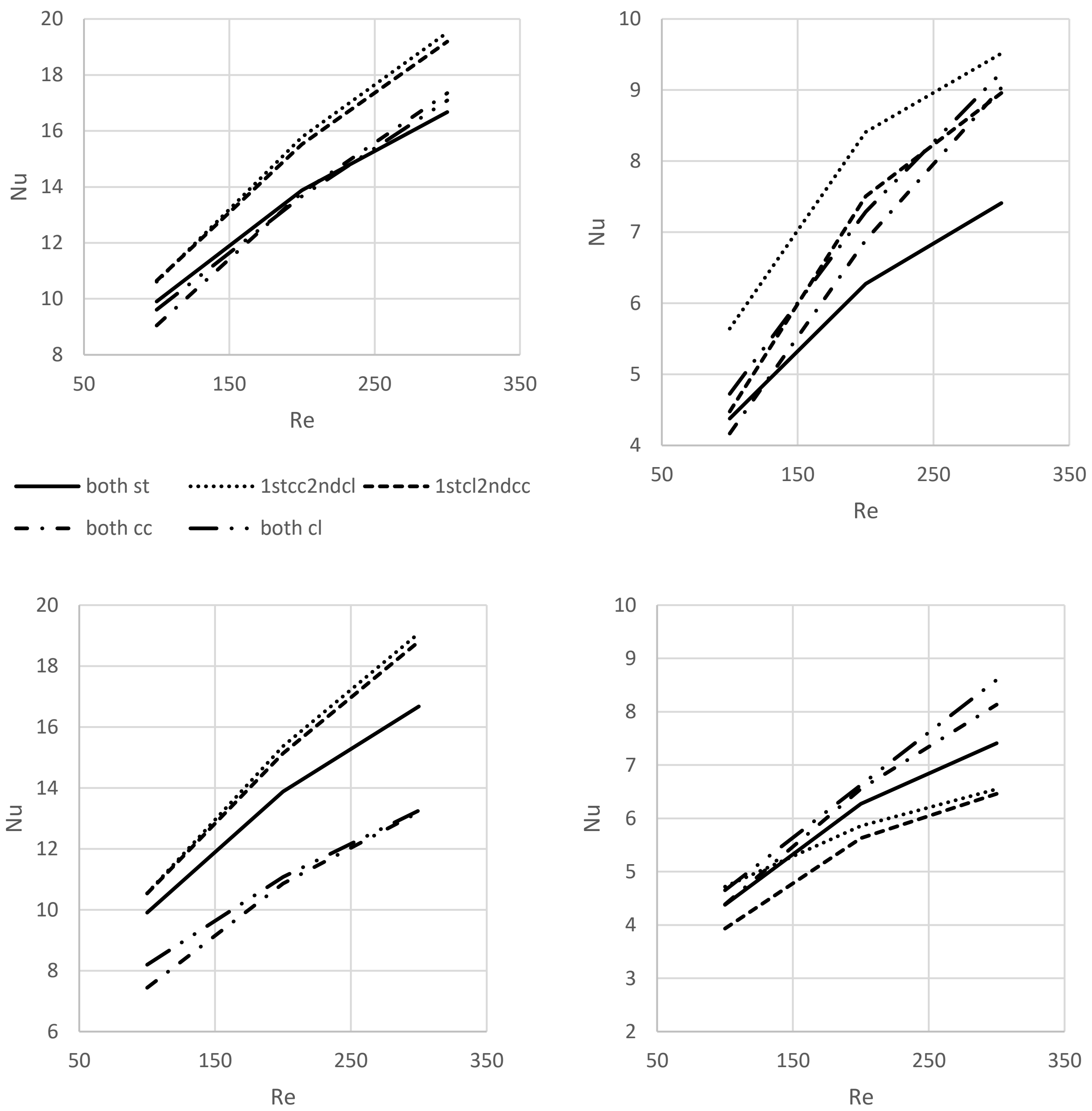

Figure 6. Nu number, Nu variations with increasing Reynolds number, Re at Gr=10^4, L_D/D =2 for different configurations.

Figure 6 shows the Nusselt number variations, *Nu* variations with increasing Reynolds number, Re at Gr=10^4, L_D/D =2. The general trend is similar in this case with at Gr=10^4, L_D/D =1.5. The maximum Nusselt Number, *Nu*, for the first cylinder is obtained as 19.19 when the first cylinder is rotating counterclockwise and the second cylinder is rotating clockwise at Re=300 and Ω=6. The maximum Nusselt Number, *Nu*, for the first cylinder is obtained as 16.6 when both of the cylinders are at stationary for Re=300 and Ω=6. The minimum Nusselt number, *Nu* is obtained as 3.93 for the case when the first cylinder rotates clockwise and the second cylinder rotates counterclockwise at Re=100 and Ω =12 in all cases mentioned in Figure 6.

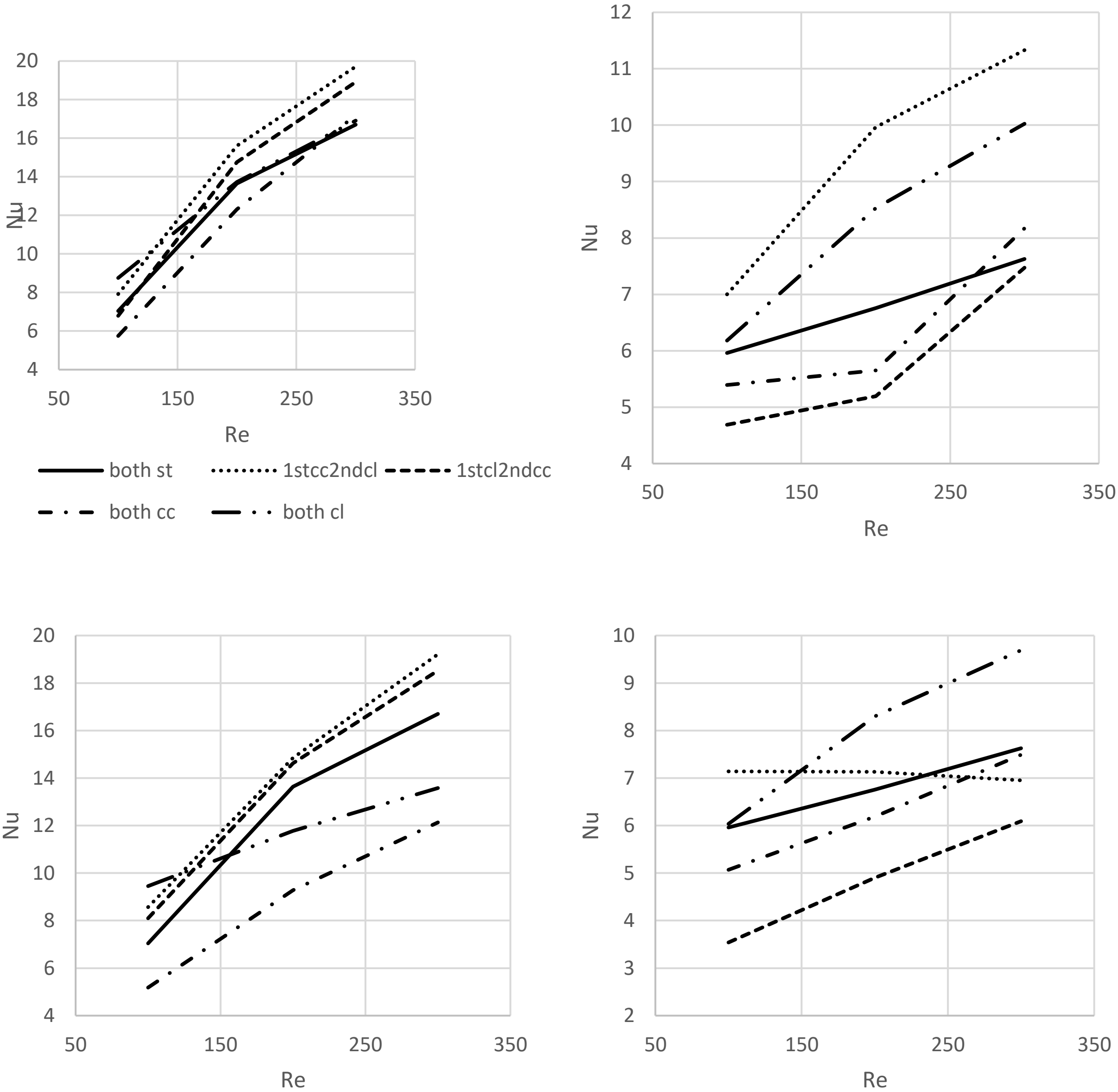

Figure 7. Nu number, Nu variations with increasing Reynolds number, Re at Gr=10^5, L_D/D =2 for different configurations.

Figure 7 shows the Nusselt number variations, *Nu* variations with rising Reynolds number, Re at $Gr=10^5$, $L_D/D=2$. The maximum Nusselt Number, *Nu*, for the first cylinder is obtained as 19.71 when the first cylinder is rotating counterclockwise and the second cylinder is rotating clockwise at Re=300 and Ω=6. The maximum Nusselt Number, Nu, for the second cylinder is obtained as 11.3 when the first cylinder is rotating counterclockwise and the second cylinder is rotating clockwise at Re=300 and Ω=6. The minimum Nusselt number, *Nu* is obtained as 3.54 belonging to the second cylinder for the case when the first cylinder rotates clockwise and the second cylinder rotates counterclockwise at Re=100 and Ω =12 in all cases mentioned in Figure 7. Whereas the minimum Nusselt number, *Nu* is obtained as 5.18 belonging to the first cylinder for the case when both cylinders rotate counterclockwise at Re=100 and Ω =12.

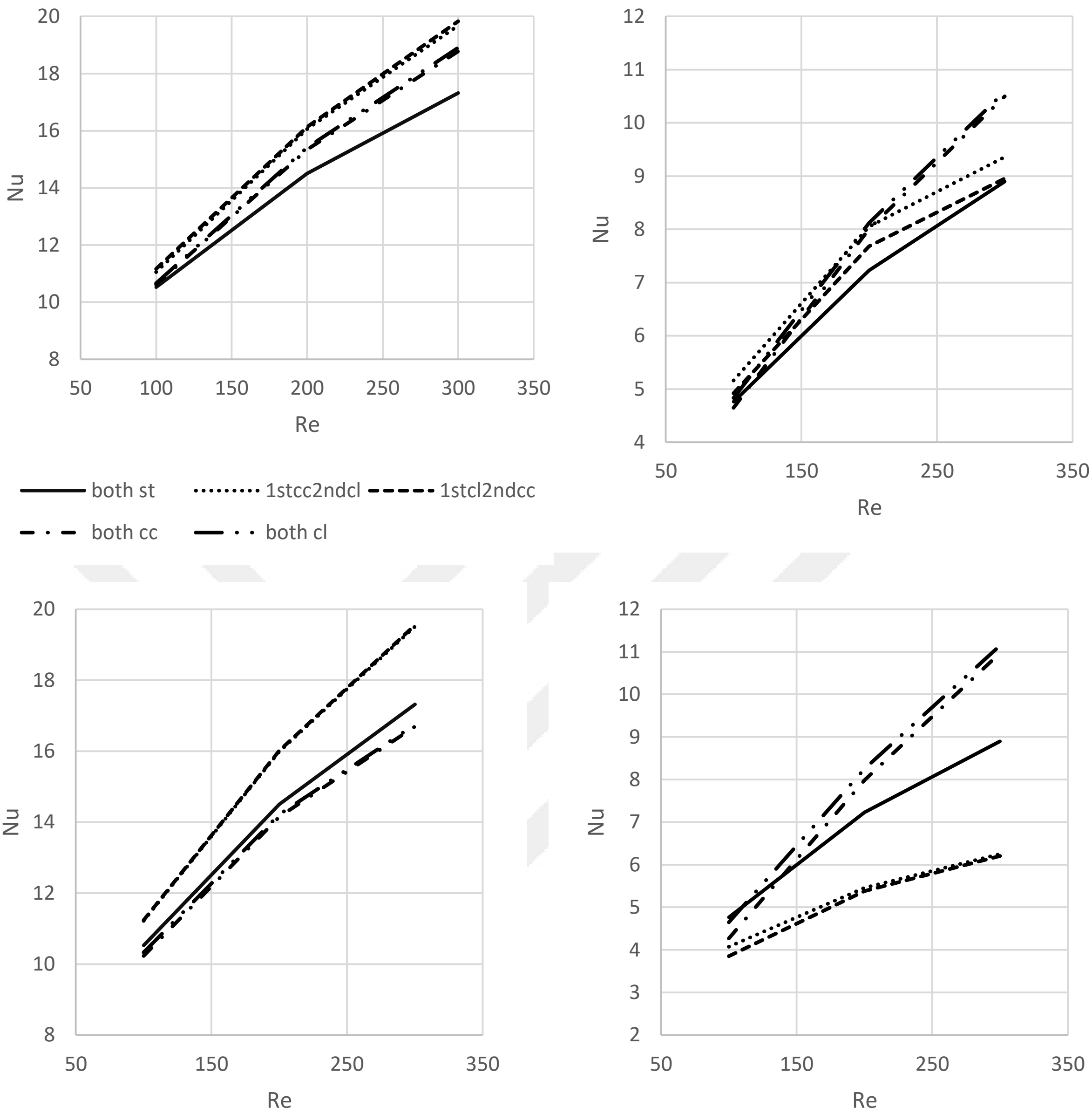

Figure 8. Nu number, Nu variations with increasing Reynolds number, Re at Gr=10^3, L_D/D =2.5.

Figure 8 shows the Nusselt number variations, *Nu* variations with rising Reynolds number, Re at Gr=10^3, L_D/D =2.5. When the first cylinder rotates counterclockwise and the second cylinder rotates clockwise, the Nusselt number associated with the first cylinder is found to be higher than when both cylinders are at stationary. The maximum Nusselt Number, *Nu*, for the first cylinder is obtained as 19.83 when the first cylinder is rotating counterclockwise, and the second cylinder is rotating clockwise at Re=300 and Ω=6. However, when both cylinders are stationary, the maximum Nusselt Number, *Nu*, for the first cylinder is 17.31 at Re=300 and Ω=6. The rotation of the cylinders increases the Nusselt number, Nu, calculated for the second cylinder in case of Ω=6. The maximum Nusselt Number, Nu, for the second cylinder is obtained as 10.58 when the cylinders rotate clockwise at Re=300 and Ω=6. Meanwhile, when both cylinders are stationary, the maximum Nusselt number is obtained as for the second cylinder is 8.95 at Re=300 and Ω=6. When the angular velocity of the cylinder increases, the Nusselt number variation trend is different with the low angular velocity cases for the first cylinder. The rotation decreases Nusselt number of the first cylinder for the case of both of the cylinder rotating clockwise or counterclockwise. However, in these cases, the Nusselt number obtained from the second cylinder increases with rotation. The maximum Nusselt Number, *Nu*, for the first cylinder is obtained as 19.54 when the first cylinder is rotating counterclockwise, and the second cylinder is rotating clockwise at Re=300 and Ω=12. The maximum Nusselt Number, *Nu*, for the second cylinder is obtained as 11.14 when both of the cylinders rotate clockwise at Re=300 and Ω=12.

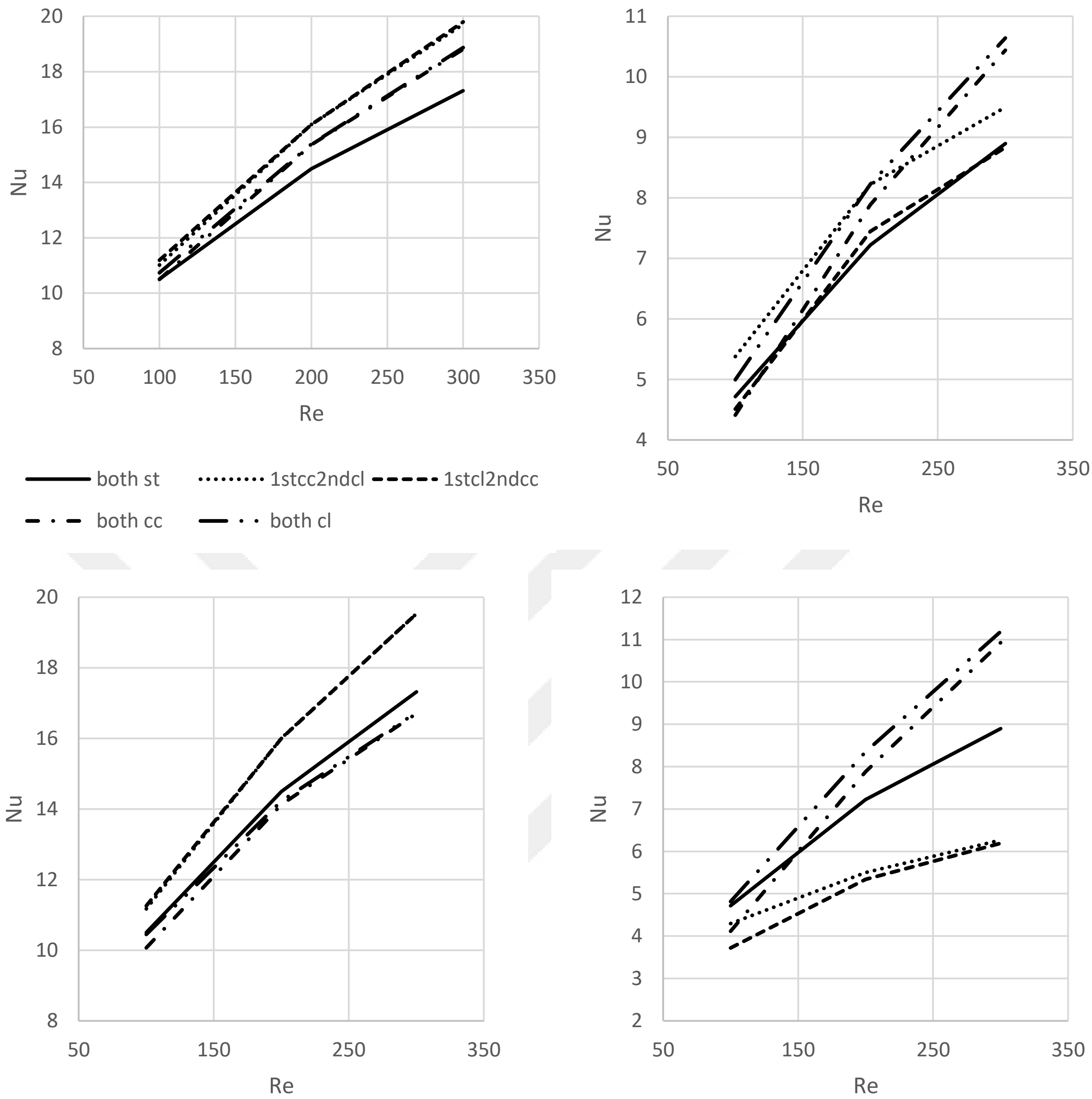

Figure 9. Nu number, Nu variations with increasing Reynolds number, Re at Gr=10^4, L_D/D =2.5 for different configurations.

Figure 9 shows the Nusselt number variations, *Nu* variations with rising Reynolds number, Re at Gr=10^4, L_D/D =2.5. the rotation of the cylinders increases Nusselt number for the first cylinder at low angular velocity cases. The maximum Nusselt Number, *Nu*, for the first cylinder is obtained as 19.80 when the first cylinder is rotating counterclockwise, and the second cylinder is rotating clockwise at Re=300 and Ω=6. However, the rotation of the cylinders varies in the trend of the Nusselt number obtained from the second cylinder. The maximum Nusselt Number, *Nu*, for the second cylinder is obtained as 10.64 when both cylinders rotate clockwise at Re=300 and Ω=6. Meanwhile the maximum Nusselt Number, *Nu*, for the second cylinder is obtained as 8.89 when both cylinders are stationary at Re=300 and Ω=6. The increase in angular velocity negatively affects the heat transfer rate from the second cylinder, especially for two cases. The maximum Nusselt Number, *Nu*, for the second cylinder is obtained as 8.89 when the both cylinders are stationary at Re=300 and Ω=12. However, if the cylinders rotate in the opposite direction of each other, the maximum Nusselt Number, *Nu*, for the second cylinder is obtained about 6.

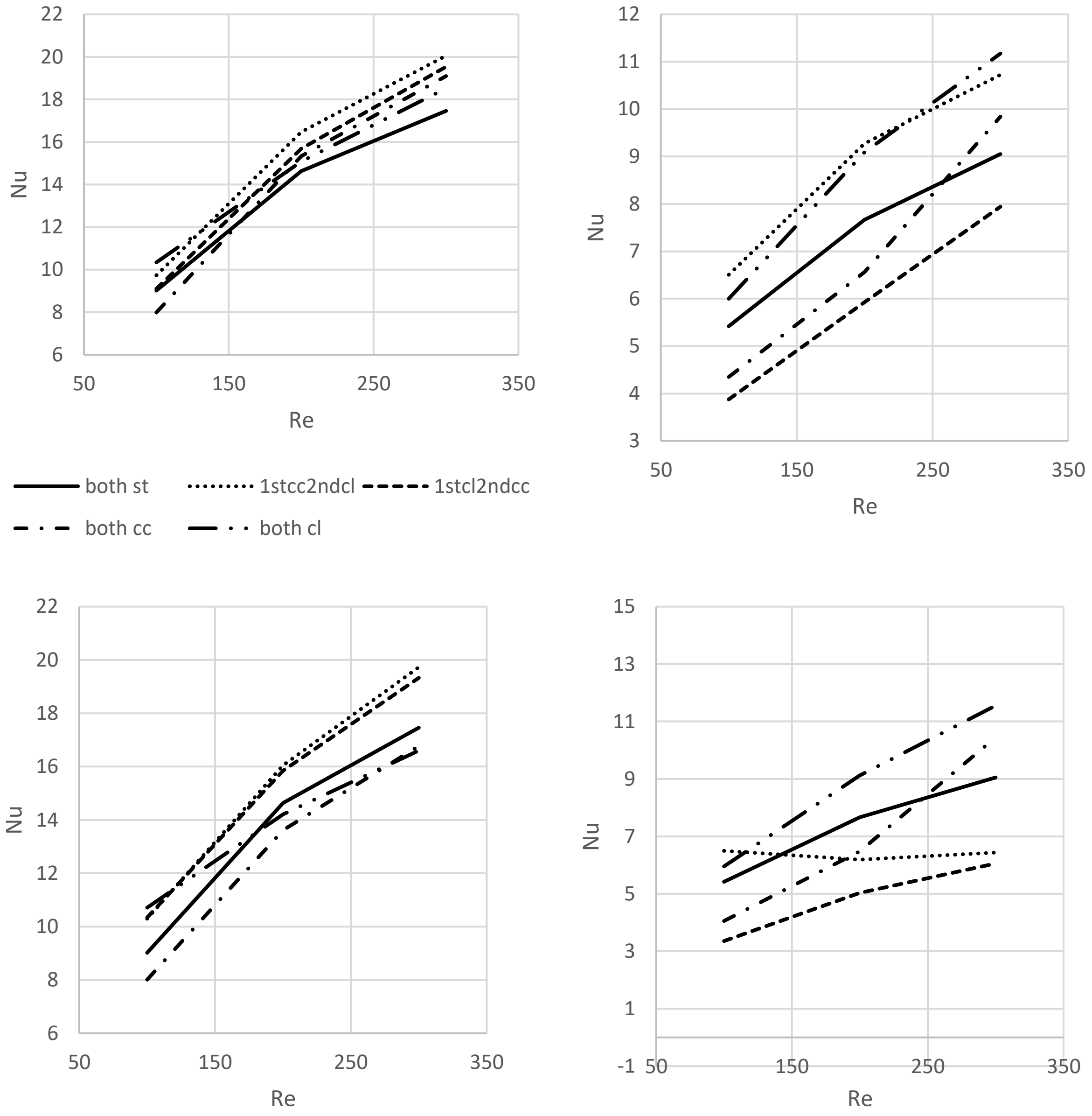

Figure 10. Nu number, Nu variations with increasing Reynolds number, Re at $Gr=10^5$, L_D/D =2.5 for different configurations.

Figure 10 shows the Nusselt number variations, *Nu* variations with rising Reynolds number, Re at Gr=10^5, L_D/D =2.5. The trend of the Nusselt number variation with Reynolds number is similar to the case of Gr=10^4, LD/D =2.5. The maximum Nusselt Number, *Nu*, for the first cylinder is obtained as 20.05 when the first cylinder is rotating counterclockwise, and the second cylinder is rotating clockwise at Re=300 and Ω=6. The maximum Nusselt Number, Nu, for the second cylinder is obtained as 11.17 when both cylinders rotate clockwise at Re=300 and Ω=6. The minimum Nusselt Number, *Nu*, for the second cylinder is obtained as 3.35 when the first cylinder is rotating clockwise, and the second cylinder is rotating counter clockwise at Re=300 and Ω=12

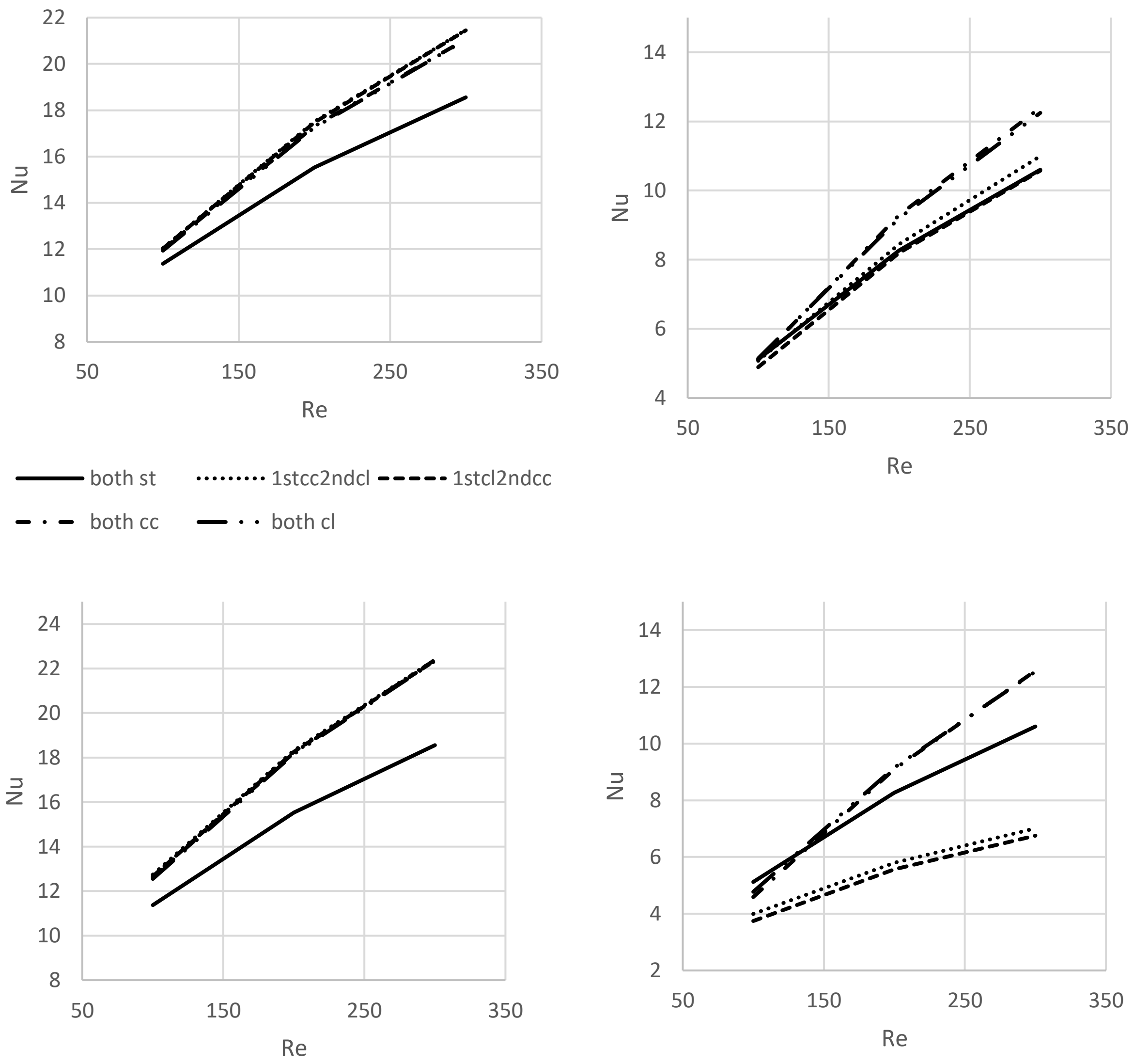

Figure 11. Nu number, *Nu* variations with increasing Reynolds number, Re at Gr=10^3, L_D/D =3 for different configurations.

Figure 11 shows the Nusselt number variations, *Nu* variations with rising Reynolds number, Re at $Gr=10^3$,10^4 and 10^5 for the configuration of L_D/D =3. This arrangement is the configuration with the largest distance between cylinders. In all mentioned LD/Ds, the highest Nusselt Number, Nu, for the first and second cylinder is obtained in this configuration. For example, the maximum Nusselt Number, *Nu*, for the first cylinder is obtained as 22.34 when both the cylinders rotate clockwise at $Gr=10^3$, Re=300 and Ω=12. The highest Nusslet number is obtained in this configuration, not only for rotating cylinders but also for cylinders at stationary in all cases. For example, the maximum Nusselt Number, *Nu*, for the first cylinder is obtained as 18.68 when both the cylinders are stationary at $Gr=10^5$, Re=300 and the maximum Nusselt Number, *Nu*, for the second cylinder is obtained as 10.62 when both the cylinders are stationary at $Gr=10^5$, Re=300.

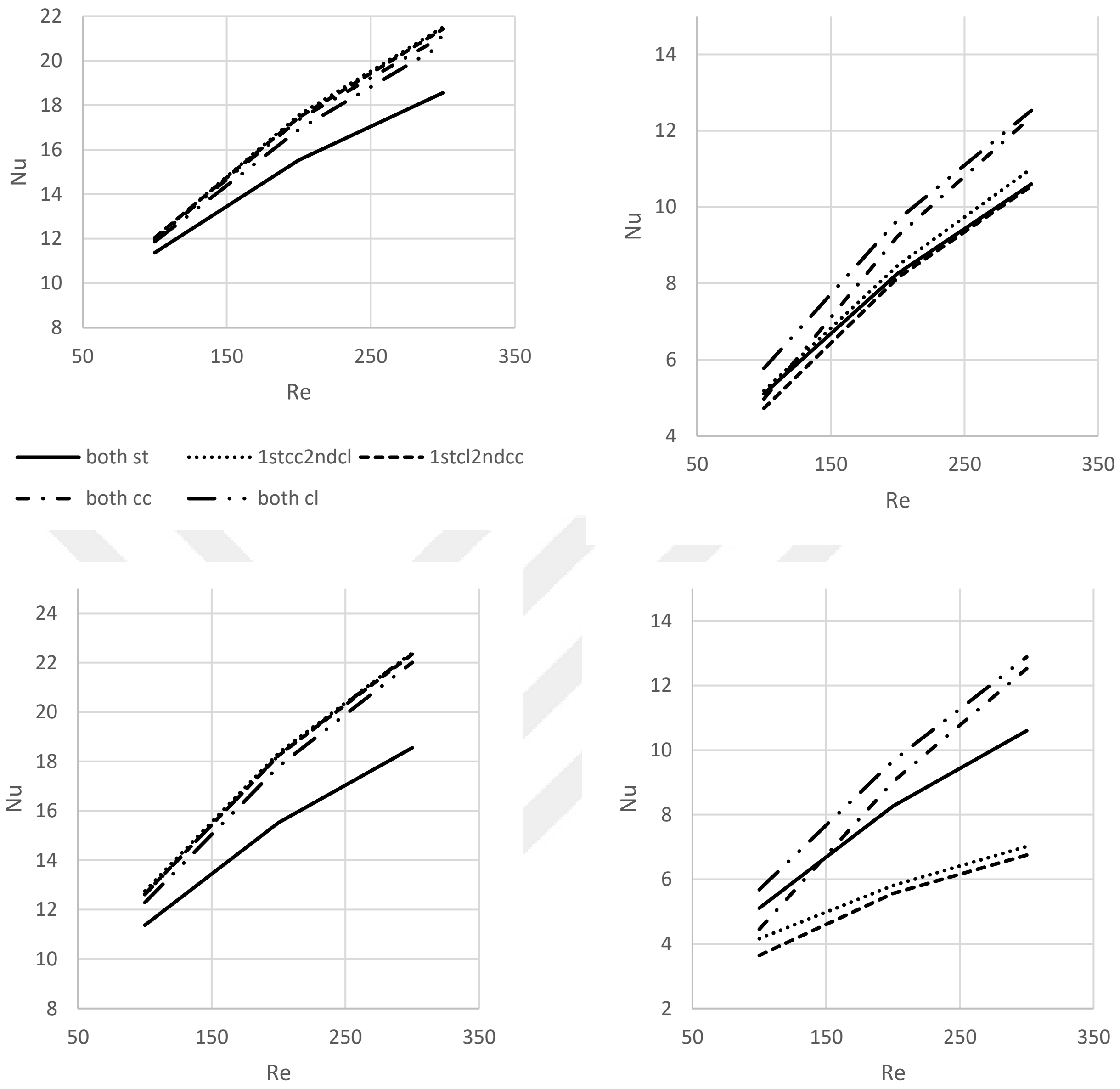

Figure 12. Nu number, *Nu* variations with increasing Reynolds number, Re at Gr=10^4, L_D/D =3 for different configurations.

Figure 12 shows the Nusselt number variations, Nu variations with rising Reynolds number, Re at Gr=10^4 for the configuration of L_D/D =3. When the first cylinder rotates clockwise and the second cylinder rotates counterclockwise, the Nusselt number associated with the first cylinder is higher than when both cylinders are at rest. The maximum Nusselt Number, *Nu,* for the first cylinder is found to be 21.09 when the first cylinder is rotating clockwise, and the second cylinder is rotating counterclockwise at Re=300 and Ω=6. Conversely, when both cylinders are rotating counterclockwise, the Nusselt number for the first cylinder is clearly lower than when both cylinders are at rest. The rotation of the cylinders increases the Nusselt number, Nu, calculated for the second cylinder in both cases. The maximum Nusselt Number, *Nu*, for the second cylinder is obtained as 10.54 when the first cylinder is rotating clockwise, and the second cylinder is rotating counterclockwise at Re=300 and Ω=6.

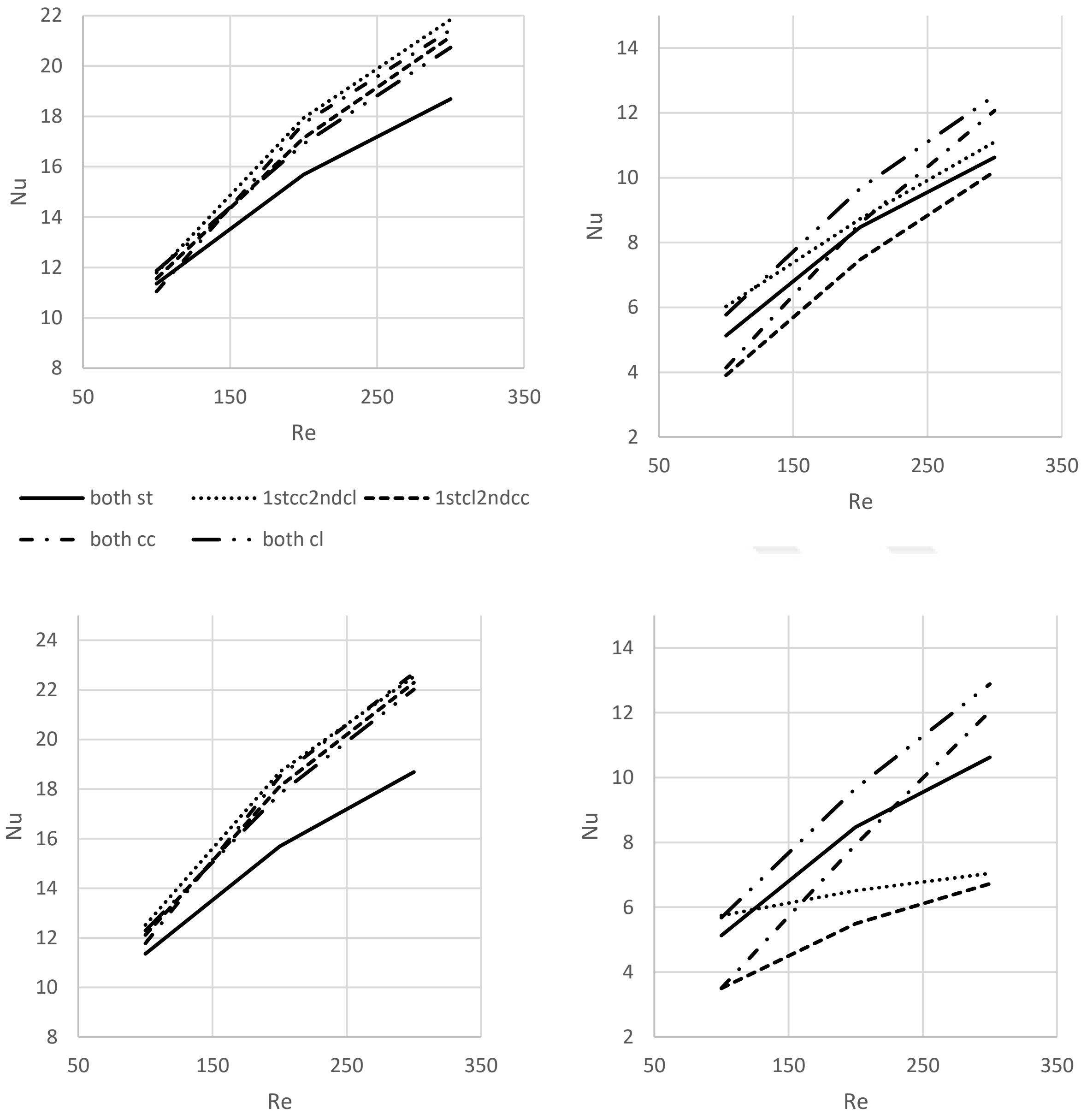

Figure 13. Nu number, *Nu* variations with increasing Reynolds number, Re at Gr=10^5, L_D/D =3 for different configurations.

Figure 13 shows the Nusselt number variations, Nu variations with rising Reynolds number, Re at $Gr=10^5$ for the configuration of L_D/D =3. When the first cylinder rotates counterclockwise and the second cylinder rotates clockwise, the Nusselt number associated with the first cylinder is found to be higher than when both cylinders are at rest. The maximum Nusselt Number, Nu, for the first cylinder is obtained as 21.42 when the first cylinder is rotating counterclockwise and the second cylinder is rotating clockwise at Re=300 and Ω=6. Conversely, when both cylinders are rotating counterclockwise, the Nusselt number for the first cylinder is clearly lower than when both cylinders are at rest. The rotation of the cylinders increases the Nusselt number, Nu, calculated for the second cylinder in both cases. The maximum Nusselt Number, Nu, for the second cylinder is obtained as 11.1 when the first cylinder is rotating counterclockwise and the second cylinder is rotating clockwise at Re=300 and Ω=6.

4.2 Flow Structures

In this part of the study, thought to be important flow structures were analyzed to assess the relations between hydrodynamics of the flow and the heat transfer mechanisms for some cases.

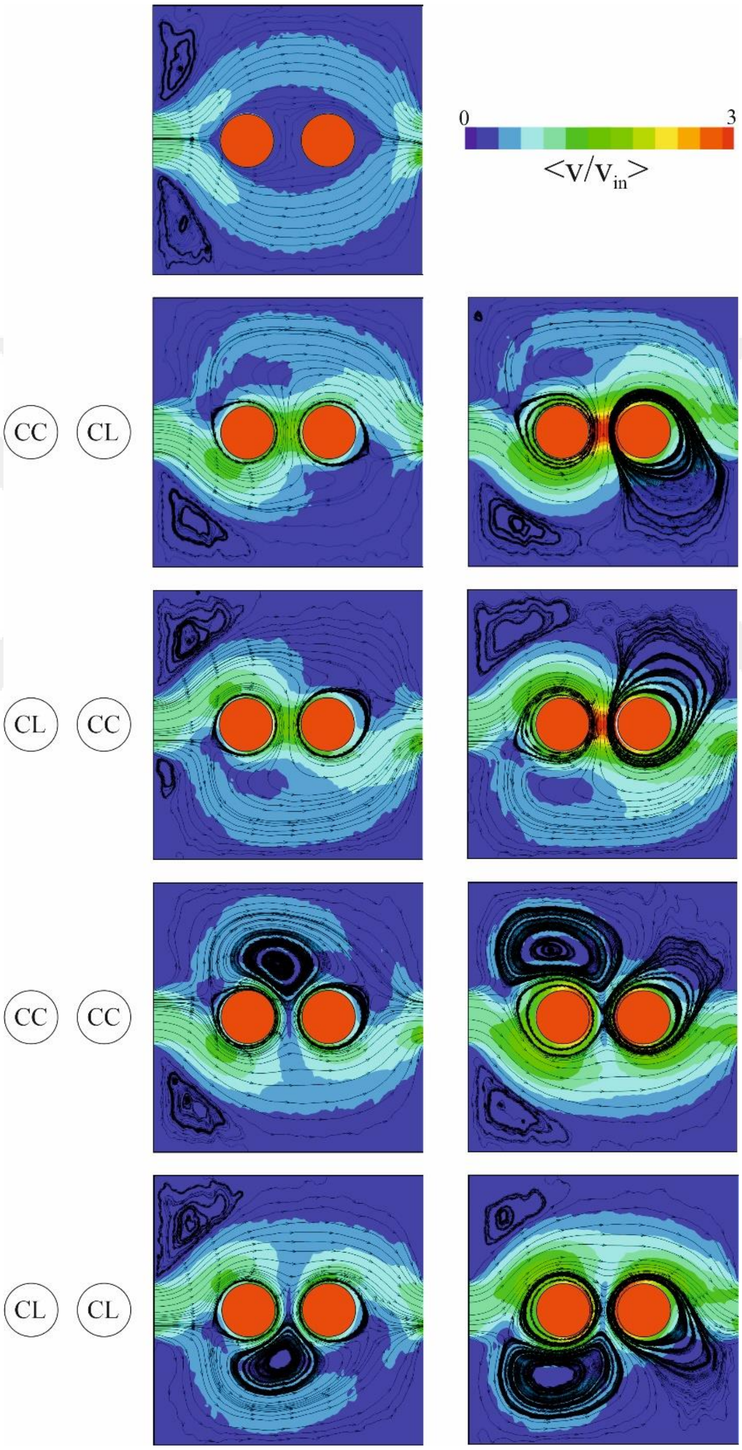

Figure 14. Time-averaged streamline topology, <Ψ>, and Normalized Time-averaged Velocity distributions <V> for different configurations at $Gr=10^3$, Re=100 and $L_D/D=1.5$

The normalized time-averaged velocity distributions superposed with the time-averaged streamline topology in the cavity with the presence of the two rotating/stationary cylinders are seen in Figure 14-25. The magnitudes of time-averaged velocity, V is normalized by the Velocity, V_{in} at the inlet of the cavity. The $<V/V_{in}>$ can be followed by the legend at the top. In Figures 14-25, the results belong to the stationary cylinder are represented at first row. As can be seen in the figures, the results presented in successive rows, the direction of rotation of the cylinders is indicated in each row. As 'CC' indicates that the cylinder rotates counterclockwise, 'CL' indicates that it rotates clockwise. Additionally, in aforementioned figures, While the cylinders in the first column have angular rotational velocity, Ω =6, the cylinders in the second column have Ω =12 rad/s. In Figure 14, the results are presented for Gr=1000, Re=100 and L_D/D=1.5. For the stationary case, the flow pattern exhibits symmetry with respect to the center of the cavity. Upon ingress through the inlet port into the cavity, the flow undergoes bifurcation. At the lower and upper sides of the cavity, symmetrically with respect to each other where the flow enters, counter-rotating vortex regions are formed. The bifurcated fluid follows closely aligned trajectories along both sides of the cylinder, subsequently exiting through the cavity's outlet port. Rotation of the cylinders in the same direction or in different directions relative to each other significantly affects the flow structure in the cavity. As seen at second row of Figure 14, the first cylinder rotates counter-clockwise and second cylinder rotates -clockwise. The recirculation region at the upper sides vanishes for both the cases Ω =6 and Ω =12. With the first cylinder rotation, it disrupts symmetry within the cavity. The main flow is directed towards the lower region of the cavity. Conversely, with the second cylinder rotation, the main flow is redirected towards the space between the two cylinders, advancing to the upper region of the cavity before exiting through the outlet port. As angular rotational velocity increases, the flow velocity at the region between cylinders increases. Additionally, the recirculation region at the lower region of the cavity expands in size. As seen in the third row of Figure 14, the first cylinder rotates clockwise, while the second cylinder rotates counterclockwise. Any recirculation region at the bottom is existed for both Ω = 6 and Ω = 12. With the rotation of the first cylinder, the symmetry within the cavity is broken. The main flow is directed toward the upper region of the cavity. Conversely, with the rotation of the second cylinder, the main flow is directed toward the cavity between the two cylinders and advances toward the upper region of the cavity before exiting the outlet port. As the angular rotation velocity increases, the flow rate in the region between the cylinders increases. In addition, the recirculation region in the upper region of the cavity expands in size. As seen in the fourth row of Figure 14, both cylinders are rotating counterclockwise. The main flow is directed toward the lower region of the cavity. As the angular rotation velocity increases, the recirculation zone at the upper part of the cavity expands in size and its focus point approaches to the inletport of the cavity. As seen in the fifth row of Figure 14, both cylinders are rotating clockwise. The flow pattern occurs as the opposite of the flow field described in the previous case, relative to the cavity center axis. The main flow is directed toward the upper region of the cavity. As the angular rotation velocity increases, the recirculation region at the lower part of the cavity expands in size and its focus point approaches to the inletport of the cavity.

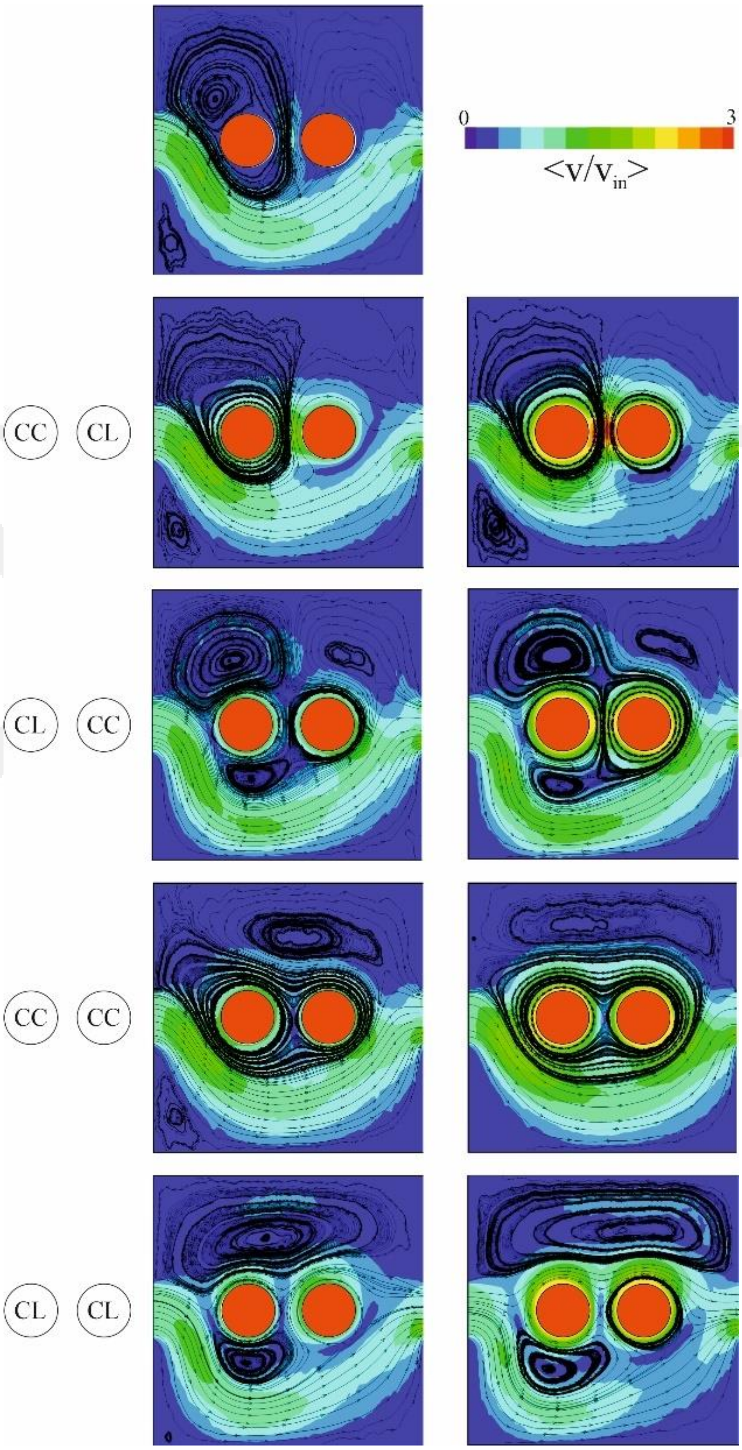

Figure 15. Time-averaged streamline topology, <Ψ>, and Normalized Time-averaged Velocity distributions <V> for different configurations at $Gr=10^5$, Re=100 and $L_D/D=1.5$

In Figure 15, the results are presented for $Gr=10^5$, Re=100 and $L_D/D=1.5$. For the steady state, the flow pattern is not symmetrical with respect to the center of the cavity due to higher Gr number, relativly. When it introduce the cavity through the inlet, the flow mostly directs to the lower part of the cavity and leaves from the outlet port. Whether the cylinders rotate in the same direction or in different directions with respect to each other significantly affects the flow structure in the cavity. As seen at second row of Figure 15, the first cylinder rotates counter-clockwise and second cylinder rotates -clockwise. As the first cylinder rotates, it brings the main flow area closer to the cylinders. With the rotation of the second cylinder, the main flow region moves towards the region between the cylinders. Moreover, as the angular rotation velocity increases, the main fluid velocity between the cylinders increases. As seen in the third row of Figure 15, the first cylinder rotates clockwise, while the second cylinder rotates counterclockwise. As the first cylinder rotates, it moves the main flow area away from the cylinders. Although the rotation effect of the second cylinder brings the main flow region closer to the cylinders, it does not affect the main flow region as much as described in the previous case. In this case, large-sized recirclation regions that rotate opposite each other occur in the upper part of the cavity. As seen in the fourth row of Figure 15, both cylinders are rotating counterclockwise. . In this case, large-sized recirclation region occur in the upper part of the cavity. As the cylinders rotate, they brings the main flow area closer to the cylinders. In fact, as rotation velocitys increase, the main flow region gets closer to the cylinders. So that part of the main flow region appears at the upper part of the cavity. As seen in the fifth row of Figure 15, both cylinders are rotating clockwise. The recirculation regions covers almost the entire upper part of the cavity for both cases such as $\Omega = 6$ and $\Omega = 12$. The small-scale recirculation zone formed due to the rotation effect of the first cylinder moves the main flow zone away from the cylinders. With the rotation of the second cylinder, the main flow region moves towards the region between the cylinders. Morever, as the angular velocity of the cylinders increases, some of the main flow region moves the upper part of the cavity. Then directs to the outport of the cavity.

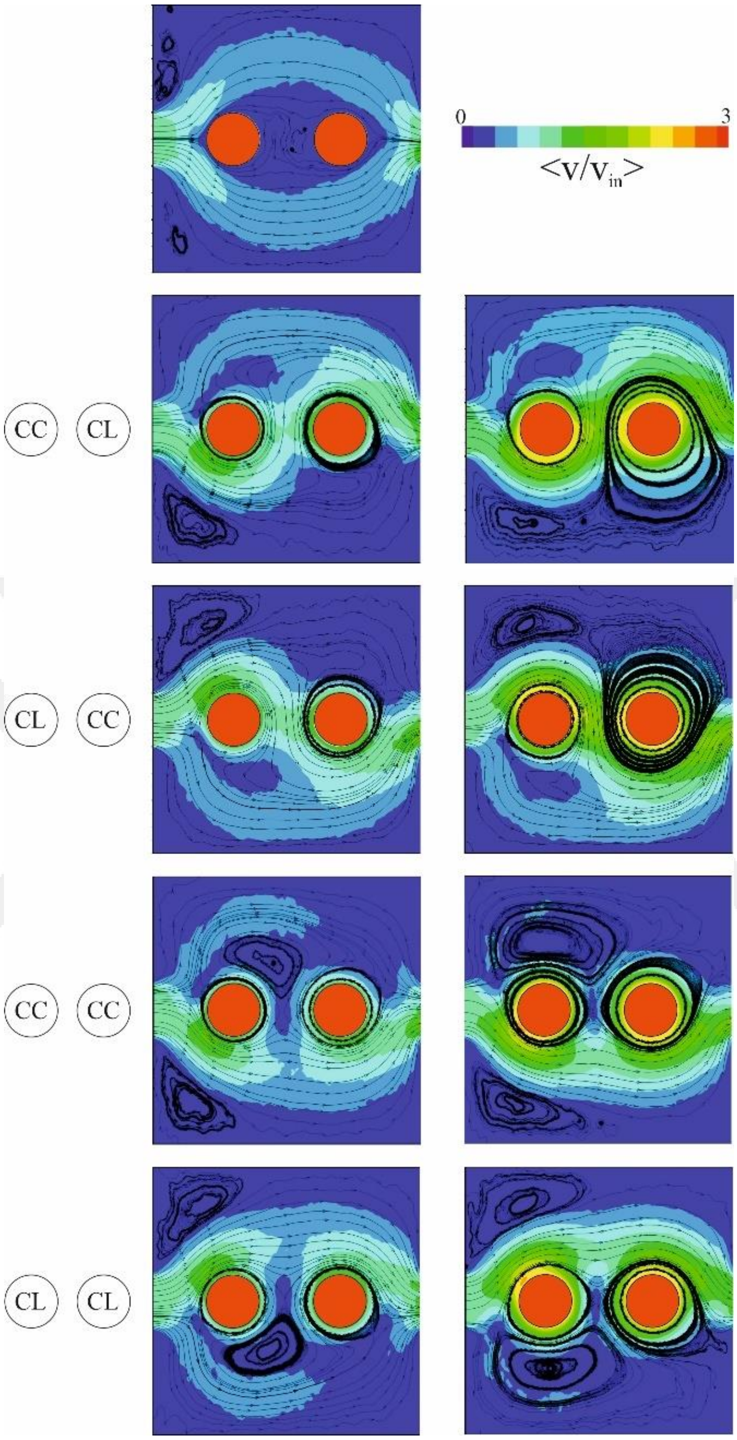

Figure 16. Time-averaged streamline topology, <Ψ>, and Normalized Time-averaged Velocity distributions <V> for different configurations at $Gr=10^3$, Re=100 and $L_D/D=2$

In Figure 16, the results are presented for $Gr=10^3$, Re=100 and $L_D/D=2$. The flow pattern shows symmetry with respect to the cavity center at steady state. The flow pattern in this instance is comparable to that of $Gr=10^3$, Re=100 and $L_D/D=1.5$. As seen at second row of Figure 16, the first cylinder rotates counter-clockwise and second cylinder rotates -clockwise. With the first cylinder rotation, it disrupts symmetry within the cavity. With the first cylinder rotation the main flow to pass through the cavity's lower part. The main flow passing between the cylinders and toward the upper part of the cavity because of the second cylinder rotating. The main flow in the cavity between the cylinders increases with increasing angular rotation velocity. In the lower part of the cavity, the recirculation zone also increases. As seen in the third row of Figure 16, the first cylinder rotates clockwise, while the second cylinder rotates counterclockwise. As the first cylinder rotates counterclockwise, the main flow field moves towards the upper part of the cylinder. The main flow area at the top, however, firstly moves to the space of of the cylinders and then moves to the outlet port from the lower part of the second cylinder when the second cylinder rotates counterclockwise. Additionally, a recirculation region is occurring at the upper part of the cavity. As seen in the fourth row of Figure 16, both cylinders rotate counterclockwise. In this case, compared to the previous case, it is observed that small-sized recirculation zones are formed in the upper and lower parts of the space.With the rotation of the first and second cylinder, the main flow moves to the lower side of the cavity. However, it is observed that with the increase in velocity, the main flow area approaches the cylinders. In this way, with the increase in velocity, recirculation regions formed in the lower and upper part of the main flow expand in size. Both cylinders rotate in a clockwise direction, as shown in the fifth row of Figure 16. The main flow zone is directed from the upper cavity to the cavity's outer port by cylinders.

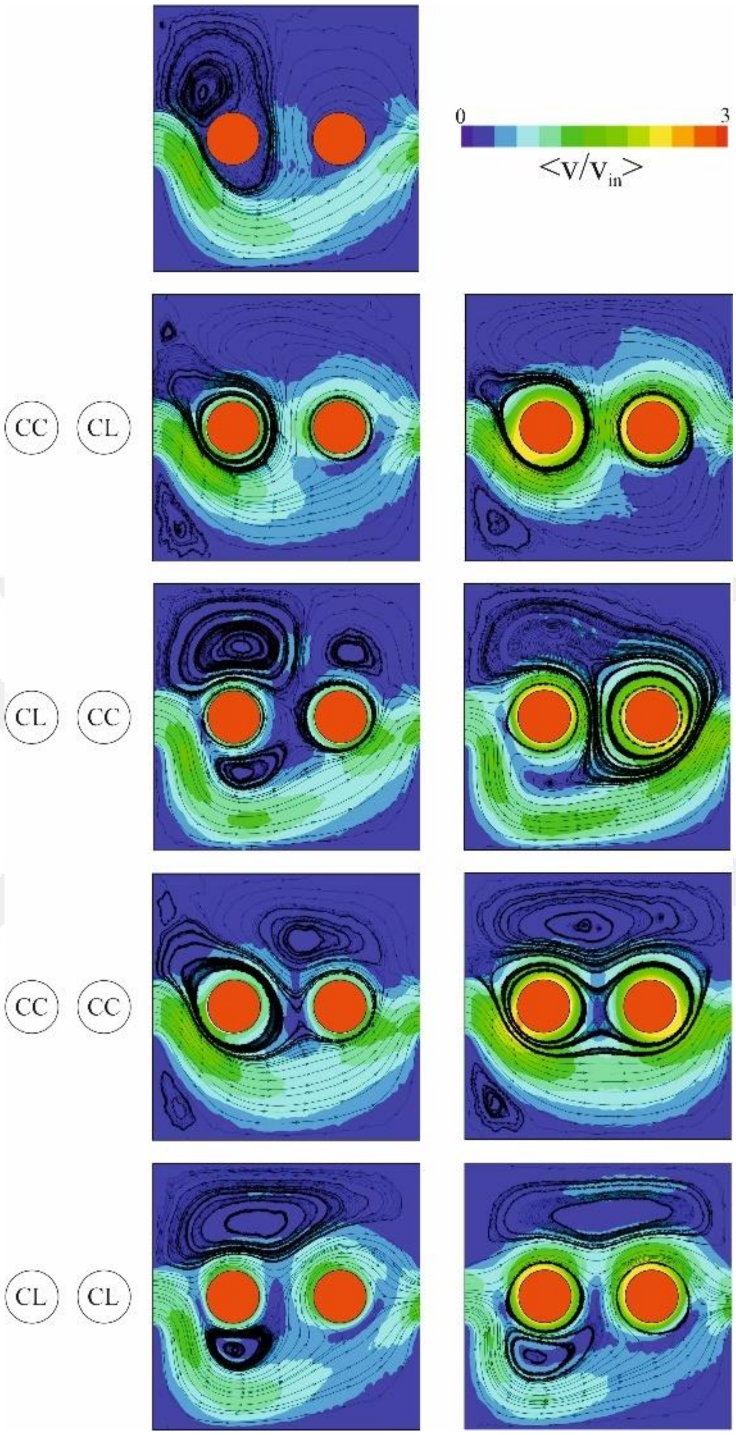

Figure 17. time-averaged streamline topology, <Ψ>, and Normalized Time-averaged Velocity distributions <V> for different configurations at $Gr=10^5$, Re=100 and $L_D/D=2$

In Figure 17, the results are presented for $Gr=10^5$, Re=100 and $L_D/D=2$. For steady state, the main flow pattern proceeds from the bottom of the cavity. The main flow field proceeds from the bottom of the cavity and exits the cavity through the outlet port. The rotation of the cylinders in the same or different directions relative to each other significantly affects the flow structure in the cavity. As seen in the figure, the recirculations region density is concentrated around the first cylinder. The first cylinder rotates counterclockwise, while the second cylinder rotates clockwise, as shown in the second row of Figure 17. The main flow field is enters and continue during the lower part of the cavity. On the other hand, when the second cylinder rotates, the main flow proceed between the cylinders and move upper part of the cavity before exits from the outlet port. The flow rate in the area between the cylinders increases with increasing angular rotation velocity. As seen in the third row of Figure 17, the first cylinder rotates clockwise and the second cylinder rotates counterclockwise. With the rotation of the first cylinder, the main flow moves away from the first cylinder with the rotation of the first cylinder. However, it was observed that with the increase in velocity, the main flow approached the cylinders again. The main flow is directed towards the lower region of the cavity. With the rotation of the second cylinder, the main flow field moves from the lower region of the cavity towards the outlet port. As the angular rotation velocity increases, the flow rate in this region between cylinders increases. In addition, compared to the stationary cylinders case, the size of the recirculation zone in the upper region of the cavity also expands. As seen in the fourth row of Figure 17, both cylinders are rotating counterclockwise. The main flow moves same like the case of stationary cylinders. With the rotation of the both cylinders, the main flow moves to the outlet port from the lower part of the cavity. The recirculation region is expands on the upper side of the cavity. Also, with the changes of the angular velocity on the cylinders effect the recirculation region around the cylinders. As you can see at the figure, increasing the angular velocity increases the main flow flied in the lower region of the second cylinder. Changing of the angular velocity also effects the recirculation region. The more the angular velocity increases, the recirculation region increase. As seen in the fifth row of Figure 17, both cylinders are rotating clockwise. Compared to the stationary cylinders, with the rotation of the both cylinders, some of the main flow moves upper and lower part of the cavity. But also the main flow concentrated at the lower part of the cavity. Increasing of the rotational velocity moves the main flow intensively to the upper part of the cavity. Before exits the outer port, the main flow moves upper and lower part of the cavity.

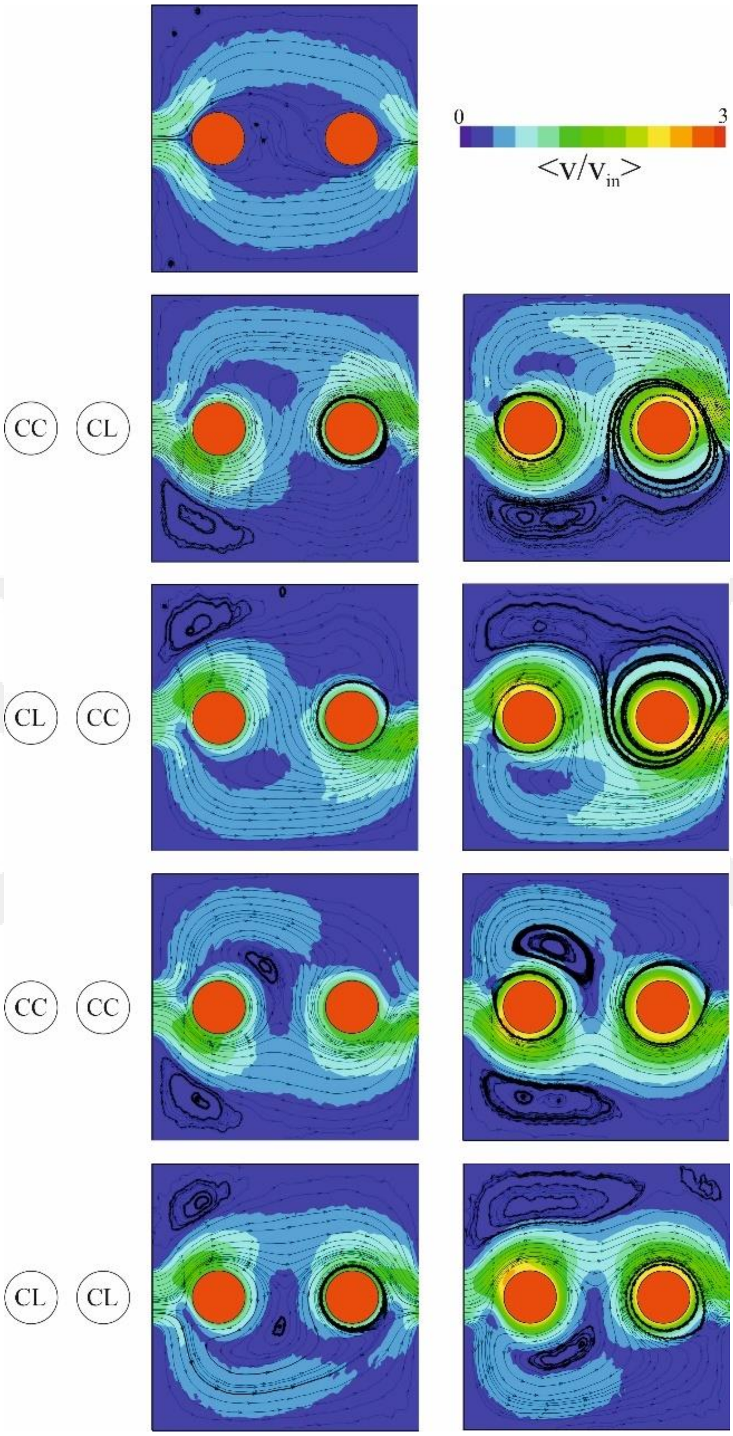

Figure 18. time-averaged streamline topology, <Ψ>, and Normalized Time-averaged Velocity distributions <V> for different configurations at $Gr=10^3$, Re=100 and $L_D/D=2.5$

In Figure 18, the results are presented for $Gr=10^3$, Re=100 and $L_D/D=2.5$. For the steady state, the flow pattern is symmetrical about the center of the cavity. The flow splits into two upon entering the cavity through the inlet port. The main flow symmetrical with respect to where the flow entered. The main flow field moves symmetrically untill the outer port of the cavity. As seen in the second row of Figure 18, the first cylinder rotates counterclockwise while the second cylinder rotates clockwise. The recirculation region is at the lower part of the cavity and also increases the recirculation regions with the increase of the rotational velocity. The main flow field moves upper and lower part of the cavity with the rotation of the first cylinder. But the flow moves intensively to the lower part. The increase of the angular velocity increases the upper part of the cavity for main flow field but also increase the intensity of the lower part of the cavity. The changes of the angular velocity effects the main flow intensity between the cylinders. As seen in the third row of Figure 18, the first cylinder rotates clockwise, while the second cylinder rotates counterclockwise. The main flow is directed toward the intensely upper part of the cavity. Also the main flow at the lower part of the cavity is move away from the first cylinder. Conversely, with the rotation of the second cylinder, the main flow is directed toward the cavity at the middle of the cylinders and than to the lower part of the cavity before exiting the outlet port. As the angular rotation velocity increases, the flow rate in this region between the cylinders increases. In addition, the recirculation region in the upper region of the cavity expands in size. As seen in the fourth row of Figure 18, both cylinders are rotating counterclockwise. The same rotational moves of the cylinders creates recirculation regions between the cylinders and the lower part of the cavity. Also, the increase of the angular velocity expands the recirculation regions. The main flow moves from the upper and lower parts of the cavity. With the rotation of the second cylinder, the main flow moves towards the lower parts of the cavity before exits the outer port. As seen in the fifth row of Figure 18, both cylinders are rotating clockwise. The recirculation regions are according to the fourth row of figure upper part of the cavity. Also we can see that the angular velocity increases the recirculation regions. The main flow slipts from the enter of the cavity to upper and lower part. But according to the angular velocity the main flow moves to the upper part of the cavity before exits the outer port.

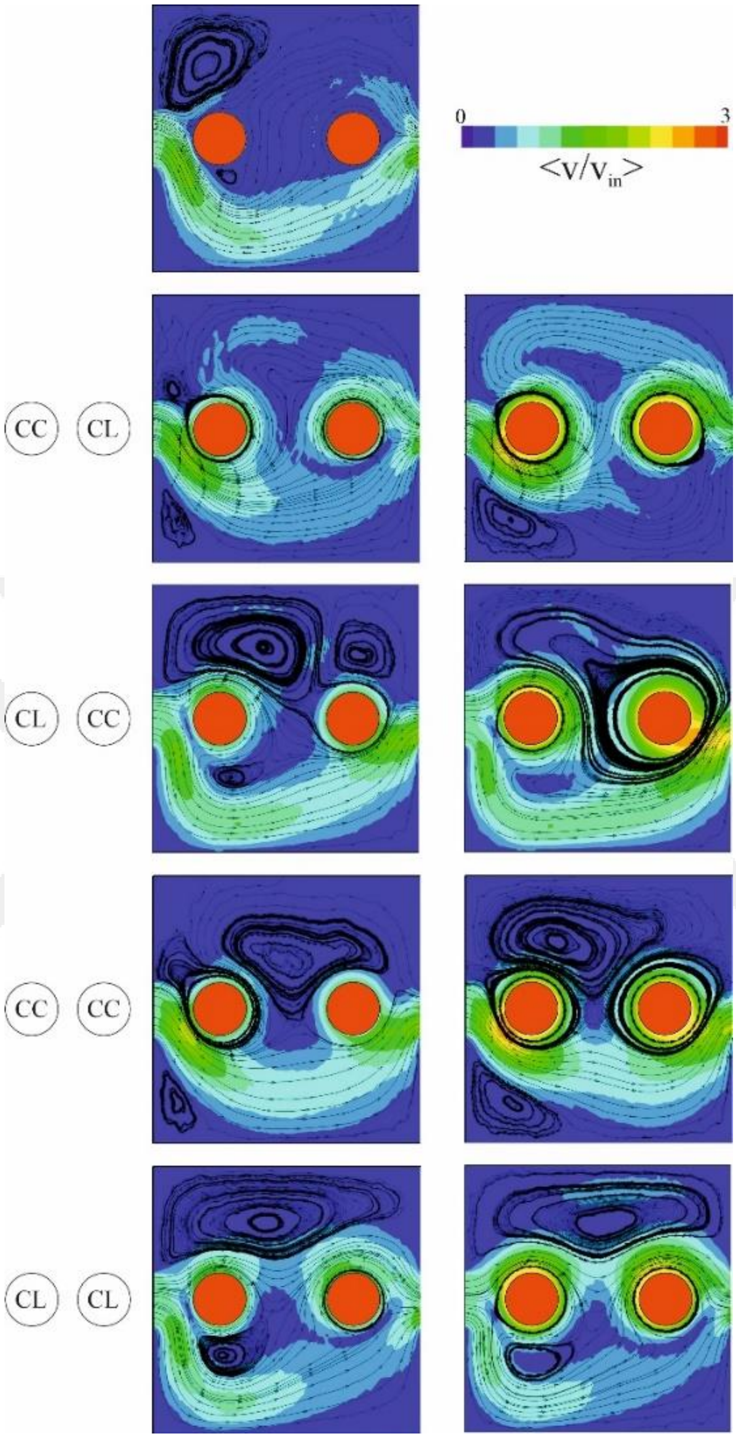

Figure 19. Time-averaged streamline topology, <Ψ>, and Normalized Time-averaged Velocity distributions <V> for different configurations at $Gr=10^5$, Re=100 and $L_D/D=2.5$

In Figure 19, the results are presented for $Gr=10^5$, Re=100 and $L_D/D=2.5$. For the steady state, the main flow is directed to the lower part of the cavity. Recirculation region are formed at the upper part of the cavity near the inlet port of the cavity. The main flow moves lower part before exits the cavity through the outlet port. As seen in the second row of Figure 19, the first cylinder rotates counterclockwise while the second cylinder rotates clockwise. The main is directed to the lower part of the cavity before exits the outer port. With increases of the angular velocity, the main flow directed from lower part to space of the cylinders, than to the upper part of the cavity before exits the outer port. In addition, the recirculation region increases with the increase of the angular velocity at the lower part of the cavity. As seen in the third row of Figure 19, the first cylinder rotates clockwise, while the second cylinder rotates counterclockwise. The main flow directed to the lower part of the cavity with the rotation of the first cylinder. The move is continue from the lower part with rotation of the second cylinder before exits the outer port. As seen in the fourth row of Figure 19, both cylinders are rotating counterclockwise. In the fourth row of figure the recirculation regions are larger than the steady state case. The rotation of the cylinders effect the recirculation regions size. Also the angular velocity increases the area of the recirculation regions. The main flow moves same like the case of steady state. However, rotation of the cylinders and angular velocity changes expands the main flow of the cavity. The more angular velocity increases, the main flow closer to the space of the cylinders. Also the main flow starts from the lower part of the cavity and exits from the lower part of the cavity before outer port. As seen in the fifth row of Figure 19, both cylinders are rotating clockwise. With the rotation of the first cylinder, the lower part of the main flow move away from the first cylinder. Than with the rotation of the second cylinder, the main flow move closer to the second cylinder. With the rotation of the cylinder the main flow directed to upper and lower part of the cavity before exits from the outer port. Also the recirculation regions are expands at the upper part of the cavity compare to the lower part of the cavity. The angular velocity effects the recirculation regions as seen in the figure.

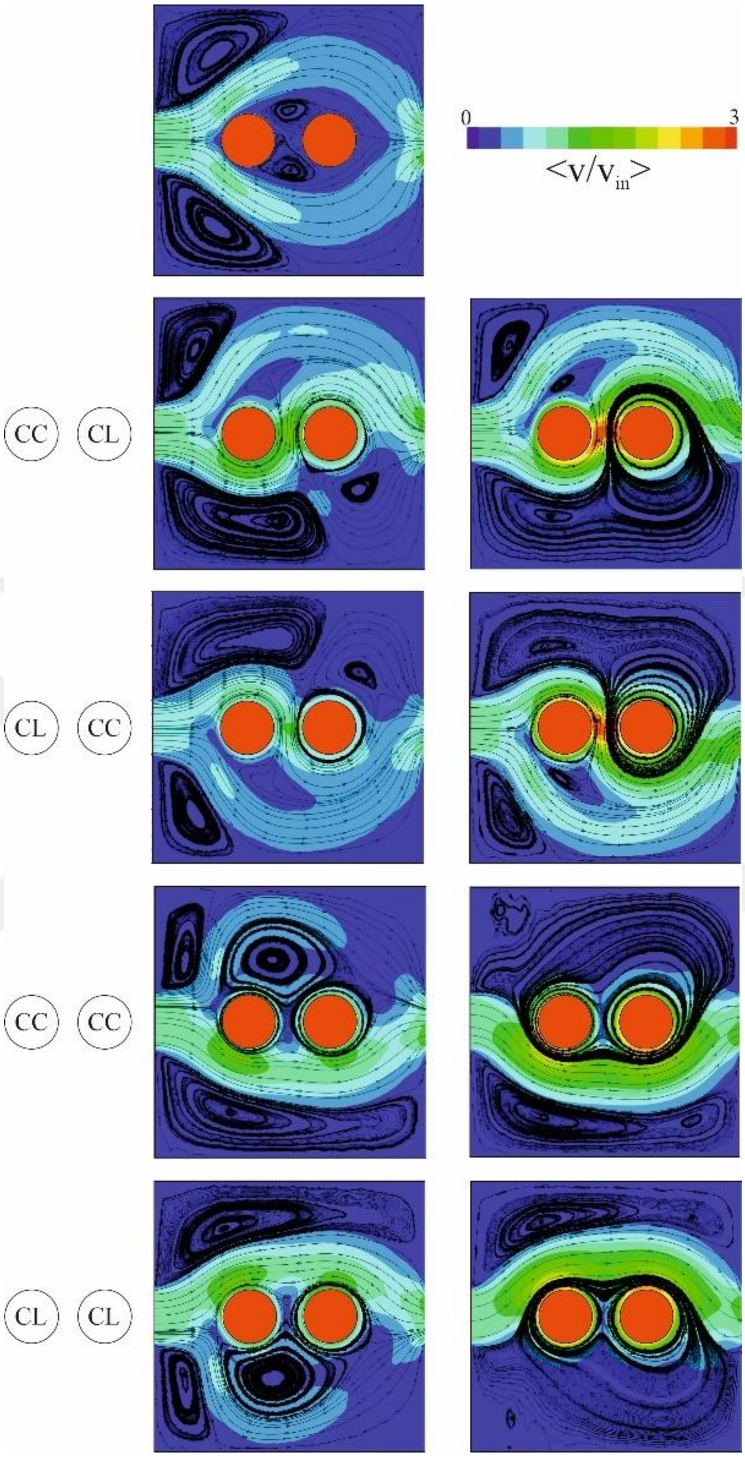

Figure 20. Time-averaged streamline topology, <Ψ>, and Normalized Time-averaged Velocity distributions <V> for different configurations at $Gr=10^3$, Re=300 and $L_D/D=1.5$

In Figure 20, the results are presented for $Gr=10^3$, Re=300 and $L_D/D=1.5$. For the steady state, the flow pattern is symmetrical with respect to the center of the cavity. As the Re rises from 100 to 300, rotational flow regions become more pronounced.The flow separates into two as it introduces the cavity from the inlet. Counter-rotating recirculation regions are formed at the upper and lower part of the cavity, which are symmetrical with respect to where the flow enters. In addition, counter rotating recirculating regions are taking place in the space between the cylinders. The main flow separated from upper and lower part of the cavity and exits outer port with the via same flow. As seen in the second row of Figure 20, the first cylinder rotates counterclockwise, while the second cylinder rotates clockwise. The main flow moves lower and upper part of the cavity. However, with the rotation of the first cylinder, the main flow moves away from the first cylinder. But the rotation of the second cylinder, the main flow gets closer. Before exits the outer port the main flow area moves upper part of the cavity. The symmetry of recirculation regions in this case are vanishes with the rotation of cylinders. With the angular velocity increases, the recirculation regions are expands at the lower part of the cavity. As seen in the third row of Figure 20, the first cylinder rotates clockwise, while the second cylinder rotates counterclockwise.The recirculation regions with respect to the rotation of the cylinders are located to the upper and lower part. The changes of the angular velocity effect the location of the recirculation regions. Increase of the angular velocity, shows us the recirculation regions move to the second cylinder and upper part of the cavity expands. With the rotation of the first cylinder the main flow moves from upper and lower part of the cavity. However, with the rotation of the second cylinder, the main flow directed to the space of the cylinders and moves lower part of the cavity before exits outer port. As seen in the fourth row of Figure 20, both cylinders are rotating counterclockwise.The main flow directed from the lower part of the cavity with respect to the rotation of the first cylinder and continue to move from the lower part of the cavity with the rotation of the second cylinder before exits the outer port. As seen in the fifth row of Figure 20, both cylinders are rotating clockwise. Compare to the steady state case, in the fifh row of figure, we can see that the main flow moves upper part of the cavity before exits the outer port.

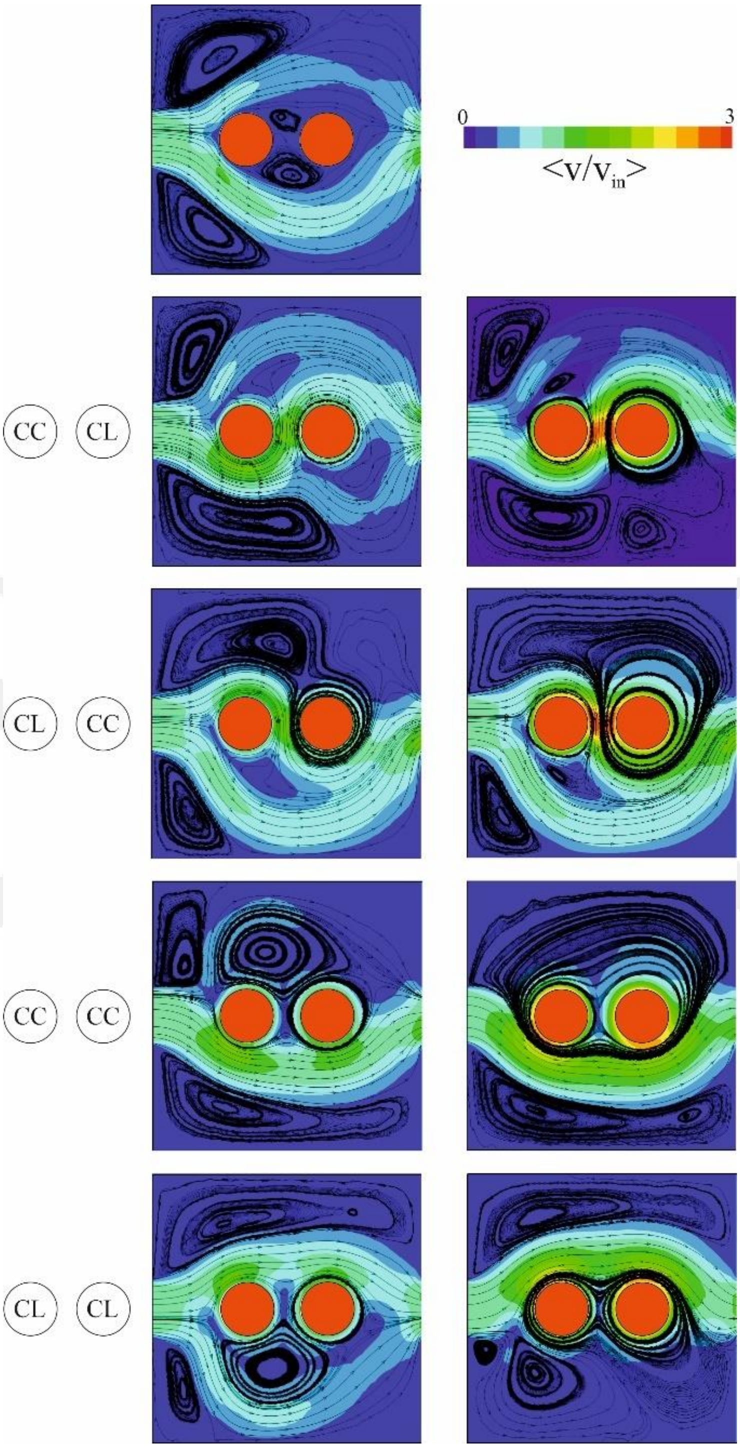

Figure 21. Time-averaged streamline topology, <Ψ>, and Normalized Time-averaged Velocity distributions <V> for different configurations at $Gr=10^5$, Re=300 and $L_D/D=1.5$

In Figure 21, the results are presented for $Gr=10^5$, Re=300 and $L_D/D=1.5$. The main flow area moves more intensively in the lower part than in the upper part and moves directed to the outer port. The recirculation regions are located at the upper and lower part of the cavity. Also small size recirculation regions located at the middle of the cylinders. The symmetry in the flow pattern with respect to the cavity center is disrupted. As seen in the second row of Figure 21, the first cylinder rotates counterclockwise, while the second cylinder rotates clockwise. This is the configuration with the highest heat transfer enhancement occurs for the second cylinder. The Nusselt number obtained from the second cylinder has almost doubled relatively to the statinary case. The recirculation regions are located at the upper and lower part of the cavity.The main flow is directed upper and lower part of the cavity. However, the increase of the angular velocity, the main flow moves lower part of the cavity. After the rotation of the second cylinder, the main flow is directed to the space of the cylinders and before exits the outer port, then the main flow is directed to the upper part of the cavity. As seen in the third row of Figure 21, the first cylinder rotates clockwise, while the second cylinder rotates counterclockwise.The recirculation regions are located at the upper part of the cavity and also small size of recirculation regions are located at the lower part of the cavity. The main flow is directed to upper and lower part of the cavity. But with the rotation of the first cylinder, the main flow move away from the first cylinder at the lower part. However, with the rotation of the second cylinder, the main flow moves closer to the second cylinder. As seen in the fourth row of Figure 21, both cylinders are rotating counterclockwise. The recirculation regions are located at the upper and lower part of the cavity.With the angular velocity increase of the second cylinder, the main flow moves closer to the second cylinder. Also the main flow moves from the lower part of the cavity before exits from the outer port. As seen in the fifth row of Figure 21, both cylinders are rotating clockwise.The main flow field moves upper and lower part of the cavity. But with rotation of the both cylinders with increase of the angular velocity, the main flow directed to the upper part of the cavity before exits outer port.

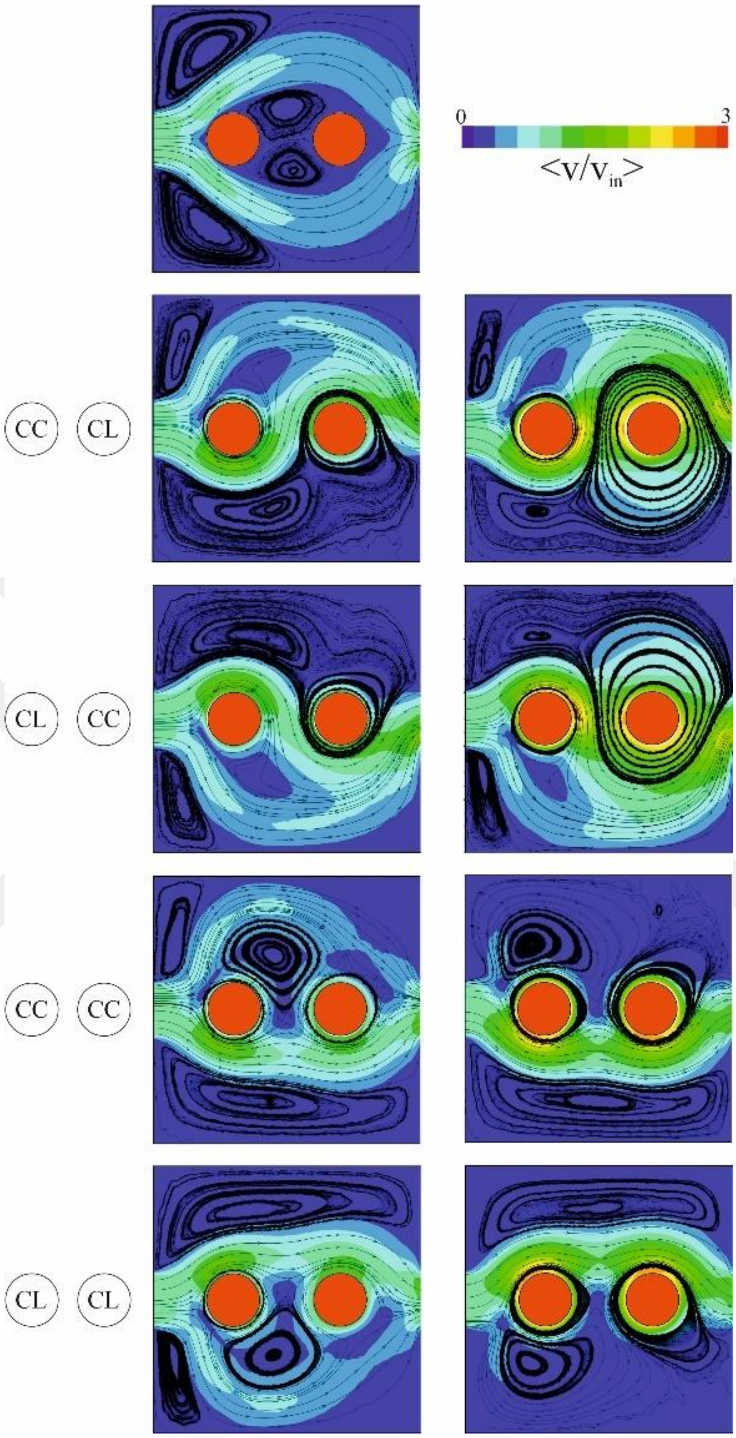

Figure 22. Time-averaged streamline topology, <Ψ>, and Normalized Time-averaged Velocity distributions <V> for different configurations at Gr=10^3, Re=300 and L_D/D=2

In Figure 22, the results are presented for Gr=10^3, Re=300 and L_D/D=2. The steady-state flow pattern is symmetrical about the center of the cavity. The main flow separates into two as it introduces the cavity from the inlet and exits outer port with the same direction. Counter-rotating recirculation regions are formed at the top and bottom of the cavity, which are symmetrical with respect to where the flow enters the center of the cylinders. As seen in the second row of Figure 22, the first cylinder rotates counterclockwise while the second cylinder rotates clockwise. The main flow separates into two when the flow enters to the inlet port. With the rotation of the first cylinder the main flow at the lower part moves to the space of the cylinders. With the rotation of the second cylinder the main flow directed to the upper part of the cylinder before exits outer port. With the rotation of the second cylinder, the main flow moves closer to the second cylinder. The recirculation regions are located at the upper and lower part of the cavity. The vortex located at the lower part of the cavity is larger than The vortex located at the lower part of the cavity. As seen in the third row of Figure 22, the first cylinder rotates clockwise, while the second cylinder rotates counterclockwise. The recirculation regions are at the upper and lower part of the cavity. At the lower part, there is an small recirculation region occurred. The main flow is directed the opposite direction of the case of second row. With the second cylinder rotation, the main flow is directed from the space of the cylinders to lower part of the cylinders before exits from the outer port. As seen in the fourth row of Figure 22, both cylinders are rotating counterclockwise. After entering the inlet port, the main flow area is divided into two. As the cylinders rotate, the main flow area in the upper part moves away from the cylinders. With increasing angular velocity, the main flow area in the upper part disappears. The main flow area continues from the lower part and proceeds to the outer port. With the increase in angular velocity, the recirculation region in the lower part also increased. As seen in the fifth row of Figure 22, both cylinders are rotating clockwise. With the increase in angular velocity, the recirculation region on the upper part remains constant. It has been observed that while the main flow field progresses in the upper and lower regions, the main flow field in the lower part moves away from the space of the cylinders with the rotation of the first and second cylinders. The main flow field progresses from the upper part with the increase in angular velocity and heads towards the exit port.

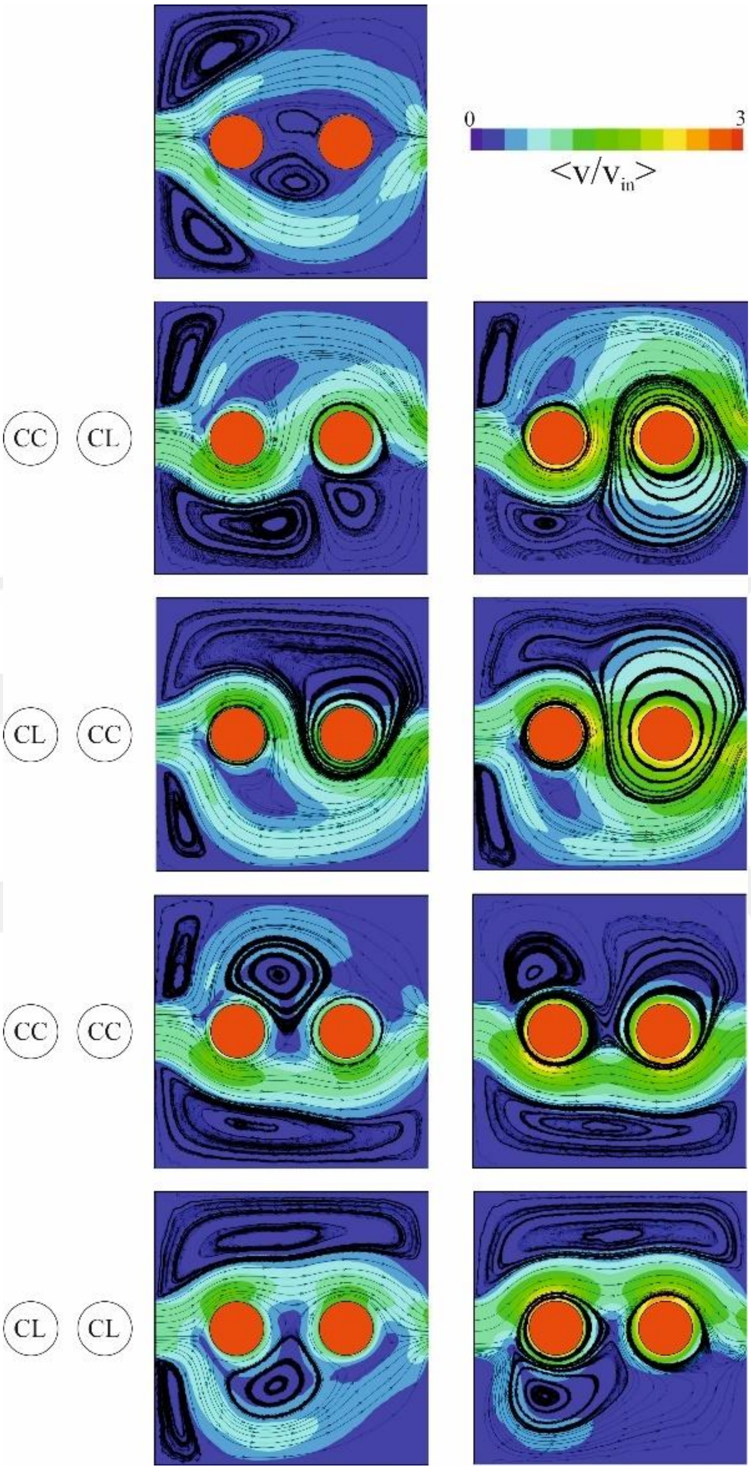

Figure 23. Time-averaged streamline topology, <Ψ>, and Normalized Time-averaged Velocity distributions <V> for different configurations at $Gr=10^5$, Re=300 and $L_D/D=2$

In Figure 23, the results are presented for $Gr=10^5$, Re=300 and $L_D/D=2$. The main flow field is divided into two regions after entering from the inlet port. However, the main flow field in the lower part has expanded compared to the main flow area in the upper part. As can be seen in figure, small-scale recirculation regions have formed in the space of the cylinders. As seen in the second row of Figure 23, the first cylinder rotates counterclockwise while the second cylinder rotates clockwise. Compared to the case with steady state cylinders, in this case recirculation regions are densely formed in the lower part of the cavity. The main flow area is divided into two regions after entering from the inlet port. It is observed that the main flow field located in the lower part of the cavity is directed to the center of the cylinders and then to the upper part of the cavity with the rotation of the second cylinder and proceeded to the exit port. The increase in rotational angular velocity in the cylinders are increased the density of the main flow area formed between the cylinders. As seen in the third row of Figure 23, the first cylinder rotates clockwise, while the second cylinder rotates counterclockwise. While the main flow area progresses in the lower and upper part with the rotation of the first cylinder, after the rotation of the second cylinder, the main flow field was directed to the lower part of the cavity. However, with the increase in angular velocity, the main flow field is also observed in the upper part of the second cylinder. As seen in the fourth row of Figure 23, both cylinders are rotating counterclockwise. The recirculation region is observed at the lower part of the cavity and near the space of the cylinders. With the rotation of the second cylinder, the main flow area formed in the upper part disappeared. In addition, it was observed that the main flow field completely is disappeared in the upper part with the increase in angular velocity. The main flow area is directed from the lower part of the cavity towards the outlet port. As seen in the fifth row of Figure 23, both cylinders are rotating clockwise. After the main flow field enters the inlet port, it continues its flow by being divided into upper and lower parts.

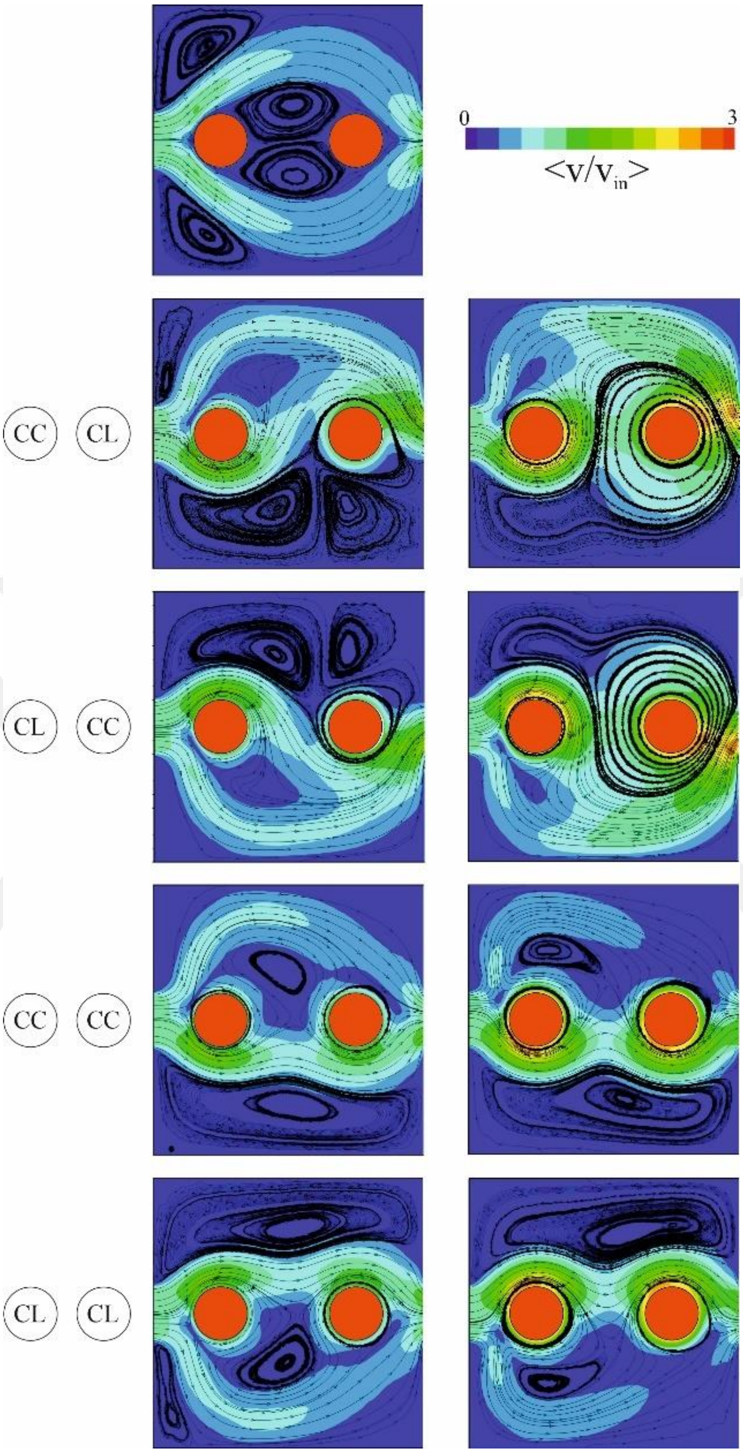

Figure 24. Time-averaged streamline topology, <Ψ>, and Normalized Time-averaged Velocity distributions <V> for different configurations at $Gr=10^3$, Re=300 and $L_D/D=2.5$

In Figure 24, the results are presented for $Gr=10^3$, Re=300 and $L_D/D=2.5$. The steady-state flow pattern is symmetric about the center of the cavity. The main flow field proceeds symmetry from the inlet port through the outlet port in the upper and lower part of the cavity. Recirculation regions occur in the upper and lower part of the entrance port of the cavity and in the center of the cylinders. As seen in the third row of Figure 24, the first cylinder rotates clockwise, while the second cylinder rotates counterclockwise. The main flow field progressed in the opposite way compared to the case in the second row. The flow field in the lower region is moved away from the cylinder with the rotation of the first cylinder and approached the second cylinder with the rotation of the second cylinder. The main flow field is directed from the lower region of the second cylinder towards the outlet port with counterclockwise rotation of the second cylinder. A recirculation region was observed in the upper part. With the increase in angular velocity, a decrease in the recirculation region in the upper part is observed. As seen in the fourth row of Figure 24, both cylinders are rotating counterclockwise. The main flow field is in the lower and upper part. Recirculation regions are observed in the lower part of the cavity and near the space of the cylinders. With the increase in angular velocity, an expansion in recirculation regions is observed. As seen in the fifth row of Figure 24, both cylinders are rotating clockwise. The main flow field moves from the upper part towards the exit port with the increase in angular velocity. With the increase in angular velocity, the recirculation region located near the space of the cylinders is observed in the lower part of the first cylinder. In addition, with the increase in angular velocity, the focus point of the recirculation region in the upper part of the cavity is concentrated in the upper part of the second cylinder.

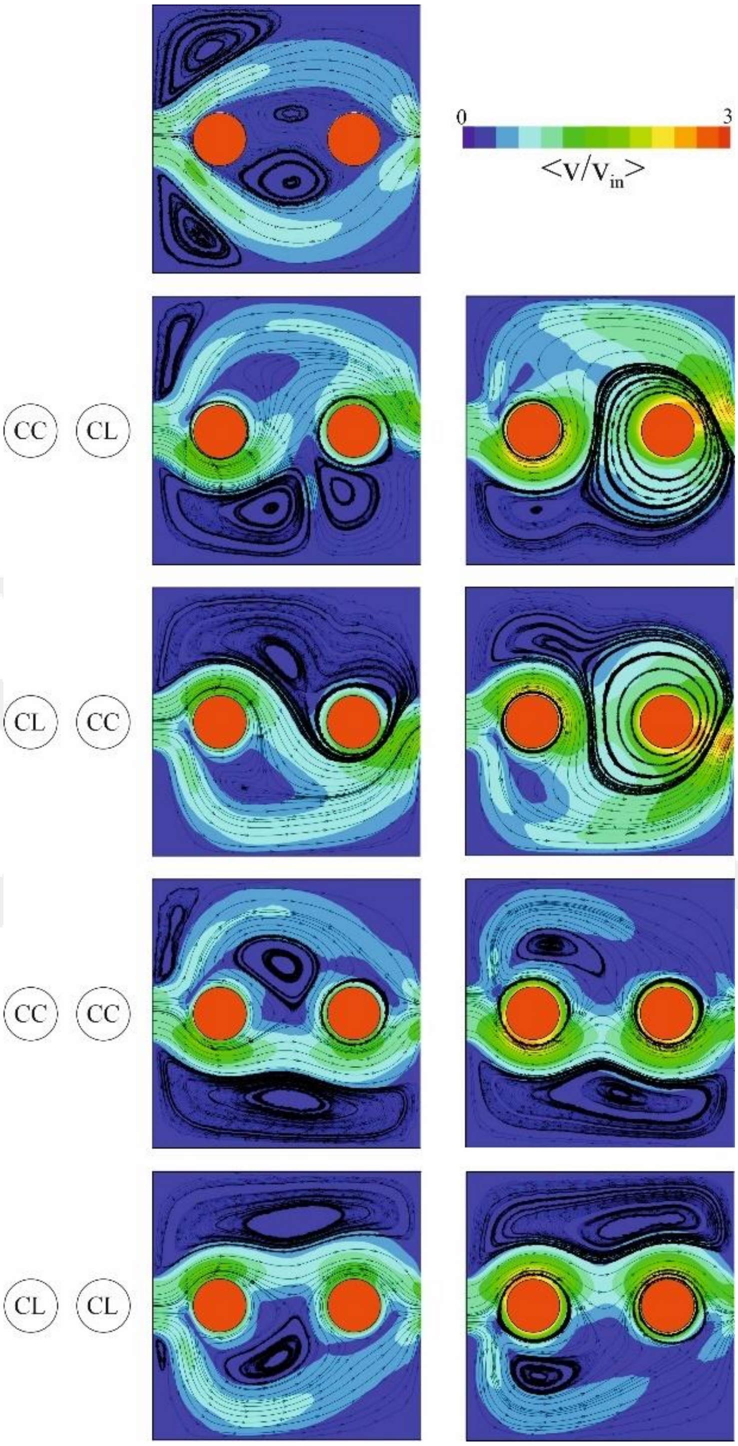

Figure 25. Time-averaged streamline topology, <Ψ>, and Normalized Time-averaged Velocity distributions <V> for different configurations at $Gr=10^5$, Re=300 and $L_D/D=2.5$

In Figure 25, the results are presented for $Gr=10^5$, Re=300 and $L_D/D=2.5$. The steady-state flow pattern is symmetric about the center of the cavity. After the main flow field enters from the inlet port, it is divided into two symmetry and proceeds to the outer port.As seen in the second row of Figure 25, the first cylinder rotates counterclockwise while the second cylinder rotates clockwise. Compared to the fixed cylinder case, in the second row case, with the rotation of the main first cylinder, the main flow field in the lower part is directed to the space of the cylinders. With the movement of the second cylinder, the main flow field is directed to the upper part moved to the exit port. As seen in the third row of Figure 25, the first cylinder rotates clockwise and the second cylinder rotates counterclockwise. The main flow field advances in the upper and lower part of the cavity. Recirculation regions are observed in the upper part of the cavity. As seen in the fourth row of Figure 25, both cylinders are rotating counterclockwise. The main flow field proceeds in the upper and lower part of the cavity. Recirculation regions occur at the lower part of the cavity and in the center of the cylinders. With the increase in angular velocity, recirculation regions near the space of the cylinders are observed in the lower part of the second cylinder. As seen in the fifth row of Figure 25, both cylinders are rotating clockwise. As the main flow field proceeds from the inlet port, it is divided into lower and upper part. With the increase in angular velocity, the main flow area in the lower part disappears and the main flow field moves from the upper part to the exit port.

CONCLUSIONS

The investigation into the mixed convection phenomena arising from two stationary and rotating cylinders situated within a cavity encompasses an evaluation of the heat transfer characteristics and flow dynamics. Employing the commercial computational fluid dynamics (CFD) software Ansys Fluent, a detailed analysis is conducted. The findings reveal that buoyancy forces exert a significant influence on the flow structures at low Reynolds numbers; However, as the Reynolds number escalates, forced convection predominates, especially in cylinders in stationary cases. For instance, with the increase of the Reynolds number from 100 to 300, the Nusselt number obtained exhibits an enhancement of 63% for the first cylinder and 107% for the second cylinder in the case of $L_D/D=3$ for $Gr=10^3$. Moreover, rotating the cylinders significantly effects the heat transfer enhancement through the cylinders in many cases. For instance, the second cylinder exhibits an improvement of about 90% when the first cylinder rotates counterclockwise, while the second cylinder rotates clockwise at Re number of 300, Gr number of $10^5$and $L_D/D=1.5$.

REFERENCES

Abo-Elkhair, R.E., Bhatti, M.M., Mekheimer, K.S. (2021). Magnetic force effects on peristaltic transport of hybrid bio-nanofluid (AuCu nanoparticles) with moderate Reynolds number: An expanding horizon, International Communications in Heat and Mass Transfer, 123,105228.

Al-Omar, S.O.O., Omar Mohammed Ali, O.M. (2023). Mixed convection from two horizontally aligned hot and cold circular cylinders in a vented square enclosure, Ain Shams Engineering Journal, 14, 102048

Azad, A.K. Hasan, M.J., Karim, M.F., Alam, E.M.M., Rahman, M.M. (2023). Rotational effect of a cylinder on hydro-thermal characteristics in a partially heated square enclosure using CNT-water nanofluid, Heliyon, 9, 12

Basem, A., (2024). Numerical analysis is being conducted to investigate the effect of Nano fluids on the melting process of phase change materials (PCMs) in a semi-cylindrical container., Applications in Engineering Science, 19, 100185.

Battira, M.M., Brahmi, C., Bessaih, R., Chadi, K. (2023). Forced convection of Cu-water nanofluid in vented square enclosure with an interior rotating hexagonal cylinder. International Journal of Heat and Technology, 41, 2, 399-406

Billah, M.M., Rahman, M.M., Sharif, U.M., Rahim, N.A., Saidur, R., Hasanuzzaman, M. (2011). Numerical analysis of fluid flow due to mixed convection in a lid-driven cavity having a heated circular hollow cylinder, International Communications in Heat and Mass Transfer,38, 1093-1103.

Costa, V.A.F., Raimundo, A.M. (2010). Steady mixed convection in a differentially heated square enclosure with an active rotating circular cylinder, International Journal of Heat and Mass Transfer, 1208-1219

Costa, V.A.F., Raimundo. A.M., (2010). Steady mixed convection in a differentially heated square enclosure with an active rotating circular cylinder, International Journal of Heat and Mass Transfer, 1208-1219.

Fluent A.N.S.Y.S (2018), "ANSYS fluent manual”

Hamzah, H, Canpolat, C., Jasim, L.M., Sahin, B. (2021). Hydrothermal index and entropy generation of a heated cylinder placed between two oppositely rotating cylinders in a vented cavity, International Journal of Mechanical Sciences, 201, 106465

Hamzah, H.K., Al-Amir, Q.R.A., Abdulkadhim, A. et al. In a Vented Square Enclosure, the Effect of a Flexible Baffle Attached to a Solid Cylinder on Mixed Convection. Arab J Sci Eng 47, 15489–15504 (2022).

Hana Ouri, H., Selimefendigil, F., Bouterra, M., Omri, M., Alshammari, B.M., Kolsi, L. (2023). MHD hybrid nanofluid convection and phase change process in an L-shaped vented cavity equipped with an inner rotating cylinder and PCM-packed bed system. Alexandria Engineering Journal, 63, 563-582

Hussain, S.H., Hussein, A.K. (2010). Numerical investigation of natural convection phenomena in a uniformly heated circular cylinder immersed in square enclosure filled with air at different vertical locations, International Communications in Heat and Mass Transfer, 37, 1115-1126.

Khalil, M., Khanafer, Ali, J., Chamkha (1998). Analysis of mixed convection in a lid-driven porous square cavity with linearly heated side wall(s), International Journal of Heat and Mass Transfer, 53,1819-1840

Khalil, M., Khanafer, Ali, J., Chamkha (1999). Mixed convection flow in a lid-driven enclosure filled with a fluid-saturated porous medium, Int. J. Heat Mass Transfer, 2465-2481

Khanafer, K., Vafai K. (2022). Double-diffusive mixed convection in a lid-driven enclosure filled with a fluid-saturated porous medium, Numerical Heat Transfer Applications, 42(5), 465–486.

Lee, J.M., Ha, M.Y., Yoon, H.S. (2010). Natural convection in a square enclosure with a circular cylinder at different horizontal and diagonal locations, International Journal of Heat and Mass Transfer,53, 5905-5919.

Mahmud, J., Rais, A. I., Hossain, R., Saha, S. (2022). Conjugate mixed convection heat transfer with internal heat generation in a lid-driven enclosure with spinning solid cylinder, Heliyon, 8, e11968

N. Alleborn, H. Raszillier, F. Durst, (1999). Lid-driven cavity with heat and mass transport, International Journal of Heat and Mass Transfer, 42, 833-853.

Oztop, H.F., Al-Salem, K. (2012). A review on entropy generation in natural and mixed convection heat transfer for energy systems, Renewable and Sustainable Energy Reviews, 16, 911-920

Selimefendigil, F., Öztop, H.F. (2023). CFD analysis and optimization of nano-enhanced phase change process in multiple port vented cavity equipped with encapsulated PCM under the combined effects of triple rotating cylinders and inclined magnetic field, Journal of Magnetism and Magnetic Materials, 575, 170716

Selimefendigil, F., Öztop, H.F. (2024). Effects of a rotating partition on mixed convection of hybrid nanofluid in a lid-driven cavity under different magnetic fields, Physics of Fluids, 4, 36, 012013

Selimefendigil, F., Öztop, H.F., (2014). Numerical study of MHD mixed convection in a nanofluid filled lid driven square enclosure with a rotating cylinder, International Journal of Heat and Mass Transfer, 78, 741-754.

Yaseen, D.T., Salih, S.M., Ismael, M.A. (2023). Effect of the lid-driven on mixed convection in an open flexible wall cavity with a partially heated bottom wall, International Journal of Thermal Sciences, 188, 108213